

20 **Abstract**

21

22 While subcortical structures such as the basal ganglia (BG) have been widely explored in
23 relation to motor control, recent evidence suggests that their mechanisms extend to the
24 domain of attentional switching. We here investigated the subcortical involvement in reward
25 related top-down control of visual alpha-band oscillations (8 – 13 Hz), which have been
26 consistently linked to the mechanisms supporting the allocation of visual spatial attention.
27 Given that items associated with contextual saliency (e.g. monetary reward or loss) attract
28 attention, it is not surprising that alpha oscillations are further modulated by the saliency
29 properties of the visual items. The executive network controlling such reward-dependent
30 modulations of oscillatory brain activity has yet to be fully elucidated. Although such
31 network has been explored in terms of cortico-cortical interaction, it likely relies also on the
32 contribution of subcortical regions. To uncover this, we investigated whether derived
33 measures of subcortical structural asymmetries could predict interhemispheric modulation of
34 alpha power during a spatial attention task. We show that volumetric hemispheric
35 lateralization of globus pallidus (GP) and thalamus (Th) explains individual hemispheric
36 biases in the ability to modulate posterior alpha power. Importantly, for the GP, this effect
37 became stronger when the value-saliency pairings in the task increased. Our findings suggest
38 that the Th and GP in humans are part of a subcortical executive control network, differently
39 involved in modulating posterior alpha activity. Further investigation aimed at uncovering the
40 interaction between subcortical and neocortical attentional networks would provide useful
41 insight in future studies.

42 **Introduction**

43 Within the domain of spatial attentional allocation, the involvement of neocortical networks
44 has been extensively studied. However, there is also growing evidence pointing to the role of
45 subcortical areas extending into higher level cognitive functions.

46 In order to efficiently operate in natural environments, our brains must rely on neuronal
47 mechanisms which selectively gate stimuli by prioritizing relevant information while
48 reducing the interference of distractors [1]. It is well established that deployment of
49 attentional resources is biased towards stimuli associated with salience (e.g. monetary reward
50 or loss), even when unrelated to the current task goals [2]. Converging evidence has shown
51 that modulations of posterior neuronal oscillations in the alpha band (8 – 13 Hz) reflect the
52 allocation of covert attention [3–5]. In particular, a selective suppression of alpha-band
53 oscillations is observed over visual areas contralateral to the attended hemifield, while a
54 relative increase occurs ipsilaterally [5]. It is now clear that the dorsal attention network
55 (DAN) plays a crucial role in the modulation of alpha band activity in spatial attention tasks
56 [6–10]; however, the involvement of subcortical regions in such modulation is yet to be fully
57 uncovered. Previous literature has indeed linked subcortical activity to cognitive control [11–
58 13], but remains to be elucidated whether subcortical areas – in coordination with the DAN –
59 exert top-down control over posterior alpha band oscillations.

60 Activity from such subcortical regions are not likely to be detectable with
61 magnetoencephalography (MEG) due to the lower sensitivity of the technique to deeper
62 structures in the brain. As an alternative, recent studies have succeeded in relating structural
63 brain properties derived from magnetic resonance imaging (MRI) to the ability to modulate
64 oscillatory brain activity, measured by MEG [14,15]. For instance, it has been demonstrated
65 that individual hemispheric asymmetries in the volume of the superior longitudinal fasciculus
66 (SLF) [8], a white matter tract connecting fronto-parietal regions, was related to the

67 individual ability to modulate alpha oscillations in visual cortical regions. Importantly, the
68 study demonstrated that subjects with greater right than left SLF volume were also the ones
69 displaying higher modulation of posterior alpha activity in the left hemisphere, compared to
70 the right (and vice versa). Through an analogous approach, we postulated that volumetric
71 asymmetries of subcortical areas would be reflected by individual interhemispheric biases in
72 the modulation of alpha oscillations during selective attention in a reward context. Basal
73 ganglia (BG), in addition to motor control, have a well-established role in reward processing
74 and salience attribution [13,16–18], although recent evidence has already pointed to their
75 functions extending into higher level cognitive processing. This notion has been initially
76 explored in animal recordings [19–24], while in humans, it has recently been suggested that
77 the BG play also a specific role in spatial attention and selection [25–27]. Consistent with
78 these lines of evidence, volumetric abnormalities related to the BG have been associated with
79 symptoms of inattention in attention deficit and hyperactivity disorder (ADHD) [28–30] and
80 with aberrant salience attribution abilities in patient with schizophrenia [31–35].
81 On the other hand, other subcortical structures such as the thalamus, have been involved in
82 the regulation of synchronized activity in the visual cortex in relation to visual attentional
83 processes [36,37]. Similarly to the premises in [8], we here assumed that a larger subcortical
84 volume would reflect higher control over alpha oscillations in a hemispheric-specific fashion.
85 To investigate this hypothesis we made use of data from a recent study that considered the
86 impact of stimuli paired with value salience on the modulation of oscillatory brain activity in
87 a covert attention task [38]. MEG data were recorded while participants performed a spatial
88 cueing task in which Chinese symbols served as targets and distractors. Prior to the
89 recordings, stimuli were paired with monetary rewards or losses. Alpha power modulation
90 was shown to be influenced by the salience of the targets and distractors, but not their valence
91 (i.e., reward and loss had the same effect). We here re-analysed these data with the aim to

92 investigate the putative role of the subcortical brain areas in biasing alpha power modulation
93 during attentional shifts to stimuli paired with value-saliency. MRI data of the same
94 participants were processed in order to estimate volumetric asymmetries of subcortical areas,
95 consistent with methods employed in previous studies on clinical and healthy population
96 [32,34,39]. We focused on identifying the link between individual volumetric asymmetries of
97 the subcortical areas and individual interhemispheric bias in the ability to modulate posterior
98 alpha oscillations. Crucially, we further examined whether this relationship was affected by
99 the degree of stimulus-value associations in the task [40].

100 **Results**

101

102 We acquired structural and electrophysiological data from 25 participants. Participants’
103 performance was tested during a covert attention paradigm, where Chinese symbols served as
104 targets and distractors (Figure 1). During a learning phase, prior to the actual task, the stimuli
105 were associated with different values (positive, negative or neutral). In the testing phase, a
106 central cue probed an upcoming contrast variation of the target, which appeared either at
107 1450 or 2350 ms, predicting its position in 95% of the trials. Participants were instructed to
108 indicate, with button press, the direction of the contrast change, which could either increase
109 or decrease with equal probability. MEG data, eye-tracking and behavioural responses were
110 acquired during the testing phase. Time-frequency representations of power were calculated
111 from MEG trials after preprocessing and artifacts rejection. Power modulation (MI) indices
112 were computed by contrasting power in trials where participants were validly cued to the
113 right (*attend right* trials) with trials where participants were validly cued to the left (*attend*
114 *left* trials) (see Eq.(1), *Materials and Methods*). As presented in the previously reported
115 results [38], we confirmed that participants displayed a clear modulation of alpha band
116 activity in parieto-occipital sensors ($MI(\alpha)$): when covertly orienting attention to the cued
117 side, alpha power decreased in the contralateral hemisphere while it increased relatively in
118 the ipsilateral hemisphere (Figure 2A). The magnitude of alpha power modulation, as
119 reflected by $MI(\alpha)$, progressively increased until the target changed contrast (Figure 2B). To
120 best quantify the modulation, we focused our analysis on the 750 ms interval immediately
121 preceding the onset of the contrast change. Next, right and left ROIs were identified as
122 clusters of symmetric pairs of sensors showing the highest alpha lateralization values (see
123 *Materials and Methods*) (i.e., sensors displaying highest interhemispheric difference in alpha
124 modulation).

125 Starting from the assumption that, to a certain extent, an inter-subject variability in the ability
126 to modulate alpha power – in absolute value – must exist in the right compared to the left
127 hemisphere (and vice versa), we sought to quantify individual hemispheric biases in the
128 ability to modulate alpha activity. To this purpose, hemispheric lateralized modulation of
129 alpha power ($HLM(\alpha)$) values were then computed for each participant by summing the
130 average $MI(\alpha)$ in the right and left hemisphere ROIs (see Eq.(2), *Materials and Methods*). As
131 a result of this computation, positive $HLM(\alpha)$ values would demonstrate that a given subject
132 was better at modulating their right, compared to left, hemisphere alpha power, while a
133 negative index would reflect higher ability to modulate alpha power on their left, compared to
134 right, hemisphere. The histogram in Figure 2B depicts the distribution of hemispheric biases
135 related to attentional modulation of alpha power. $HLM(\alpha)$ indices ranged from about -0.1 to
136 0.1 (i.e. a 20% variation) but they were normally distributed around zero across participants
137 (Shapiro Wilk, $W = .958$, $p = .392$).

138

139 *Volumetric asymmetry of basal ganglia in relation to hemispheric lateralized alpha*
140 *modulation*

141 The next step was to determine whether the biases in the ability to modulate left versus right
142 hemisphere alpha ($HLM(\alpha)$) was related to individual hemispheric lateralization of
143 subcortical structures. A semi-automated segmentation tool implemented in FMRIB's
144 Software Library (FSL), was used to estimate volumes for the left and right subcortical and
145 limbic structures, namely: Globus Pallidus (GP), Nucleus Accumbens (Acb), Caudate
146 Nucleus (CN), Putamen (Pu), Hippocampus (Hpc), Amygdala (Am) and Thalamus (Th). We
147 then calculated the hemispheric lateralized volumes (LV) for each set of structures (see
148 *Materials and Methods*, Eq.(3)). Positive (or negative) LV_s values, for a given participant,
149 indicated whether a specific substructure s was larger in the right compared to the left

150 hemisphere (and vice versa). Further analysis revealed that, over subjects, the Acb and Th
151 were significantly left lateralized ($z = -3.78, p = 1.56 \times 10^{-4}$ and $z = -3.59, p = 3.28 \times 10^{-4}$,
152 respectively; two-sided Wilcoxon signed rank test), whilst the CN was right lateralized ($z =$
153 $2.97, p = .003$). For the other substructures, no significant lateralizations were identified.
154 These significant lateralization biases in the Acb, Th and CN are of potential interest but will
155 not be further considered in the context of this study. Given the volumetric variability in the
156 set of substructures considered for the segmentation protocol, we performed a cross
157 correlation analysis between the different substructures, including left and right volumes, to
158 query about whether there might be a bias in the segmentation protocol. No significant effects
159 were found (positive or negative correlations, all p -values > 0.688 ; highest negative
160 correlation $R = -.084$) indicating that, if a given structure is larger for a given subject, this
161 doesn't imply a bias in the segmentation protocol (e.g. to the expense of neighbouring,
162 allegedly smaller areas).

163 To investigate whether individual subcortical asymmetries (LVs, as defined in Eq. (3))
164 predicted differences in hemispheric lateralized modulation of alpha power ($HLM(\alpha)$), we
165 implemented a GLM, where LV indices were included as multiple explanatory variables for
166 the response variable (individual $HLM(\alpha)$). A significant regression was found: when
167 considering the grand average of all conditions, a linear combination of the subcortical LVs
168 was able to explain $HLM(\alpha)$ values ($F_{7,17} = 3.37$, $p = .019$, adjusted $R^2 = .409$). When
169 assessing each predictor individually, only the beta coefficients for LV_{GP} and LV_{TH} were
170 found to be significantly higher than zero (partial correlation: $p = .004$ and $p = .028$) (Figure
171 4A). Hence, when controlling for the other explanatory variables in the model, only GP and
172 TH asymmetry (LV_{GP} , LV_{TH}) significantly contributed to explain biases in hemispheric
173 lateralized alpha band modulation ($\beta = 1.768$ and $\beta = 1.924$, respectively). The independent
174 contribution of GP and TH lateralization is visible in Figure 4B,C showing the partial
175 regression plots for LV_{GP} and LV_{TH} in relation to the $HLM(\alpha)$ values. We conclude that
176 hemispheric biases in GP and TH volume are predictive of the individual abilities to
177 modulate left versus right hemisphere alpha. Precisely, subjects presenting a larger GP
178 volume in the left hemisphere compared to the right, also displayed a higher ability to
179 modulate alpha power (in absolute value) in the left visual hemisphere compared to the right
180 (and vice versa); the same association holding for the Th in relation to $HLM(\alpha)$ values.

181

182 *Hemispheric asymmetry of globus pallidus correlates selectively with power modulation in*
183 *the alpha band*

184 In order to better interpret the GLM results, we assessed whether the linear relationship
185 arising from the model was restricted to the alpha band: to this end, a non-parametric
186 approach was implemented to further explore the LV_{GP} and LV_{TH} in relation to $HLM(\alpha)$.
187 This method allows circumvention of the multiple comparison problem over frequency and

188 time points by evaluating the full low-frequency spectrum (2-30 Hz) from -750 to 0ms [41].
189 We therefore conducted a cluster-based permutation test using a dependent samples
190 regression t -statistic to evaluate the effect (linear association between $LV_{GP/TH}$ indices and
191 HLM over all frequencies) at the sample level. A p -value of .05 was chosen for thresholding
192 the t -statistic of the permutation distribution and a critical value corresponding to $\alpha =$
193 .025 (two tailed) was considered for the cluster-level regression test statistic. As depicted in
194 Figure 5A, we observed a significant cluster ($p = .004$) extending for the entire 750 ms
195 window of interest (i.e., when covert attention was deployed to the cued stimulus before the
196 contrast changed), which confirmed a positive linear association (positive t -value) between
197 LV_{GP} asymmetry and hemispheric lateralized modulation (HLM) of power constrained to the
198 alpha frequency range. When applying the same analysis to the Th asymmetry in relation to
199 HLM, no significant clusters of sensors were identified.

200

201 *Hemisphere specific relations between alpha modulation and GP asymmetry.*

202 Given the specific association found between LV_{GP} and $HLM(\alpha)$, arising from the previous
203 analysis, we decided to further investigate the hemisphere-specific influence of GP
204 volumetric asymmetry on alpha modulation indices. For this purpose, we sought to compare
205 average left and right hemisphere $MI(\alpha)$ s of participants according to the direction of GP
206 lateralization. This was done by means of median split of the LV_{GP} distribution, hence
207 resulting in two subgroups, that either had a bias towards a larger left than right GP volume
208 or vice versa (see *Materials and Methods*). A topographical representation of $MI(\alpha)$ values
209 together with a bar plot of $MI(\alpha)$ averaged across right and left hemisphere ROIs per each
210 subgroup is shown in Figure 1S. Consistent with the GLM results, participants with a larger
211 right than left GP, also displayed a higher modulation of alpha band (in absolute value) in the
212 right hemisphere compared to the left. Given that the assumption of normality, necessary to

213 perform a mixed-effect ANOVA, was not met for the distribution of $MI(\alpha)$ indices in the two
214 subgroups, we implemented a non-parametric cluster-based permutation test to compare the
215 $MI(\alpha)$ between the two aforementioned subgroups (averaged across specific time and
216 frequency band of interest), employing an independent sample t-test score, and then
217 comparing it with the resulting permutation distribution. This allowed us to explore whether
218 there was a hemispheric-specific difference in the two subgroups in the extent of absolute
219 alpha modulation. The test indicated a significant cluster of sensors over right posterior
220 channels ($p = .027$), hence including the previously defined right ROI and denoting a
221 significant difference in the right hemisphere absolute alpha modulation ($MI(\alpha)$) between the
222 two subgroups. These results might suggest that the linear association arising from the GLM
223 (Figure 4A, B) in relation to the association between LV_{GP} and $HLM(\alpha)$, was largely driven
224 by right hemisphere alpha modulation. We conducted the analogous analysis performing a
225 median split of the distribution of LV_{TH} indices. In that case we did not find interhemispheric
226 dominance in alpha modulation indices related to lateralization of the thalamus in the right
227 compared to left hemisphere.

228

229 *The involvement of globus pallidus and thalamus in relation to stimulus-value associations*

230 Crucially, we aimed at assessing whether the level of value-saliency occurrences (VO) in a
231 given trial influenced the association between the structural and functional lateralization
232 indices arisen from the GLM. We first calculated $HLM(\alpha)$ (see Eq.(2), *Materials and*
233 *Methods*) values for each participant, separately for the three VO levels, namely two, one and
234 zero value saliency occurrences (see *Materials and Methods*). We then examined Pearson
235 correlations between $HLM(\alpha)$ and LV values for both GP and Th, which showed a positive
236 significant β in the model, across the three levels considered (Figure 6). LV_{GP} significantly
237 correlated with $HLM(\alpha)$ only in trials where both target and distractors had value-saliency

238 (two VO) ($r = .68, p = 1.75 \times 10^{-4}$; Figure 6A). This denotes that, in trials with two value-salient
239 items presented, participants exhibiting a right lateralized GP volume, also displayed a
240 stronger alpha modulation in the right compared to the left hemisphere, and vice versa. LV_{GP}
241 did not significantly correlate with $HLM(\alpha)$ when only one or none of the stimuli presented
242 were associated with a salient value ($p = .144$ and $p = .314$, respectively; Figure 6A).
243 In order to statistically quantify the influence of the stimulus-value association on the
244 relationship between LV_{GP} and $HLM(\alpha)$, we compared *robust correlations* in the three
245 conditions according to the bootstrap method described in [42] for dependent overlapping
246 correlations (see *Materials and Methods*). The correlation between LV_{GP} and $HLM(\alpha)$ in
247 trials with two occurrences of value-saliency, significantly differed both from the condition
248 characterized by one (95% CI [.106, .672]) and zero occurrences (95% CI [.125, .897]). This
249 confirmed that the association between lateralized GP volume and alpha modulation bias
250 significantly increased as a function of the number of value-salient occurrences in the task
251 (Figure 6B). We performed the same analysis in order to assess whether value-saliency
252 occurrences mediated also the association between LV_{TH} and $HLM(\alpha)$. When considering the
253 correlation indices in the three conditions separately, no significant linear relationship was
254 found between the two indices (Figure 7A). Also in this case, when comparing robust
255 correlations between the three conditions, according to the same method above, no significant
256 difference was found. This suggested that the relationship between thalamus volumetric
257 lateralization and alpha modulation arising from the model in Eq.(3), was not driven by the
258 number of value-salient occurrences in the task.

259

260 *Behavioural analysis*

261 We also investigated whether subjects displayed a spatial bias in task performance,
262 irrespective of the value-saliency levels. To this end we performed a paired t-test to assess

263 whether participants' performance differed between left and right cued trials, in both reaction
264 times (RT) and accuracy measures. No behavioural spatial bias was found neither in RT
265 ($p=.341$) nor in accuracy ($p=.572$) values. Secondly, we examined whether value-salient
266 occurrences (VO) levels, modulated participants' behavioural performance.
267 We then compared mean RT and accuracy for the three VOs levels (see *Materials and*
268 *Methods*). There were no statistically significant differences between the three groups, as
269 determined by one-way ANOVA, in RT ($F_{(2,72)}=.004, p=.995$) (Figure 8A) nor in accuracy
270 ($F_{(2,72)}=.003, p=.996$) (Figure 8C). We then tested whether a behavioural spatial bias occurred
271 across value saliency occurrences (i.e., whether subjects displayed a difference in RT or
272 accuracy asymmetry across VOs). We computed measures of behavioural asymmetry in
273 accuracy (BA_{ACC}) and reaction times (BA_{RT}) (see Eq.(5), *Materials and Methods*).
274 Analogously to the method used to compute $HLM(\alpha)$, we created asymmetry indices for
275 every subject by contrasting behavioural measures for *attend right* with *attend left* trials. As
276 such, a positive BA_{RT} would indicate that subjects were faster when cued to the left compared
277 to the right hemisphere, and vice versa. Similarly, positive BA_{ACC} indices reflected higher
278 accuracy when cued to the right compared to the left hemisphere. With the method
279 aforementioned, we performed a one-way ANOVA to assess whether a significant difference
280 in behavioural bias occurred across the three VO conditions. Neither BA_{RT} nor BA_{ACC} values
281 significantly differed across VOs ($F_{(2,72)}=.191, p=.826$ and $F_{(2,72)}=.669, p=.515$, respectively)
282 (Figure 8B, 8D). With the aim of determining a potential link between lateralized indices of
283 behavioural performance and the anatomical (LVs) and functional ($HLM(\alpha)$) lateralization
284 indices of interest, we employed three separate GLMs to assess whether a linear combination
285 of BA_{RT} and BA_{ACC} values could explain LV_{GP} , LV_{TH} and/or $HLM(\alpha)$ indices. Neither LV_{GP}
286 nor LV_{TH} could be explained by the behavioral lateralized measures ($F_{1,23}=.18, p=.834$,
287 adjusted $R^2=-.07$ and $F_{1,23}=.16, p=.849$, adjusted $R^2=-.07$). The same result held for the

288 prediction of $HLM(\alpha)$, yielding also in this case no significant regression coefficients
289 ($F_{1,23}=1.17$, $p=.33$, adjusted $R^2=-.01$).

290 Last, we investigated whether individual behavioral spatial biases could be accounted for by
291 a combination of the other measures examined. To this end, we considered all subcortical
292 LV_S and $HLM(\alpha)$ indices and specified them as regressors in a general linear model (see
293 Eq.(6), *Materials and Methods*), in order to determine whether they could explain biases in
294 RT and accuracy (BA_{RT} and BA_{ACC}). No significant regression was found which could
295 account for BA_{RT} indices ($F_{8,16}=.85$, $p=.570$, adjusted $R^2=-.05$) nor for BA_{ACC} indices
296 ($F_{8,16}=1.07$, $p=.429$, adjusted $R^2=-.023$, respectively). (Figure 2S). The lack of a relationship
297 between spatial bias in task performance and functional and structural hemispheric
298 lateralization indices is likely explained by the orthogonalization of attentional orienting and
299 stimulus-value associations, in line with the null findings in [38].

300 **Discussion**

301 The aim of this study was to investigate the involvement of subcortical structures in
302 modulating spatial attention to stimuli associated with contextual salience. In particular, we
303 investigated volumetric measures of subcortical structures in relation to the ability to
304 modulate visual alpha oscillations in the framework of an attentional task with a reward
305 component [43,44]. We made use of a previous dataset in which alpha activity was
306 modulated by both spatial attention and value-saliency associations[38]. We first observed
307 that volumetric lateralization of subcortical areas explained individual differences in the
308 ability to modulate interhemispheric alpha power. More specifically, participants exhibiting a
309 right lateralized GP also had a better ability to modulate posterior alpha oscillations in the
310 right compared to left hemisphere, and vice versa. The same association held for the
311 relationship between Th and alpha modulation. For the GP, we were able to show how this
312 association was significantly constrained to the alpha frequency band. Importantly, we
313 showed that the association between GP and alpha hemispheric lateralized modulation
314 increased as a function of value-saliency occurrences in the task: the correlation between GP
315 lateralized volume and alpha modulation asymmetry was significantly higher in trials where
316 both target and distractor were represented by a salient item (reward or loss) as compared to
317 one or zero salient items. With respect to the Th and its association to interhemispheric alpha
318 power modulation, no relation to saliency was found. To the best of our knowledge, this is
319 the first finding relating individual volumetric differences in BG and thalamus to the
320 modulation of posterior alpha oscillations.

321

322 *Subcortical areas and alpha synchronization*

323 Our first finding is in line with a growing body of literature demonstrating a subcortical
324 involvement in high level cognitive functions, such as conscious perception [45], working

325 memory performance [46], cognitive control [47–49] and attentional control [50,51]. Specific
326 to attentional control, we showed that volumetric asymmetry of the subcortical areas
327 considered predicts individual biases in the ability to efficiently allocate attention towards a
328 cued target, as indexed by interhemispheric modulation of alpha power. This is strong
329 evidence in favor of a subcortical involvement in attentional processing, given the well-
330 established role of neuronal synchronization in the alpha band into the selective gating of
331 relevant information during visuospatial covert attention tasks [52,53]. Although the
332 functional association between BG and cognitive control in the context of reward has been
333 already investigated [54,55], we here provide novel insights into the involvement of
334 subcortical regions in the modulation of posterior alpha oscillations.

335

336 *Pulsed inhibition*

337 A well-recognized function of the BG is to inhibit or promote cortical activity via
338 GABAergic signalling, through the globus pallidus pars interna (GPi), one of its major output
339 structures [56,57] (see below for a discussion of potential pathways). The BG might then
340 exercise its influence by applying control over activity in the prefrontal cortex or it might
341 directly coordinate posterior regions (as reflected by its relationship to alpha power
342 modulation during reward processing). Our results suggest that individual differences in GP
343 volume lateralization may correspond to interhemispheric variability in GABAergic
344 signalling and thus reflect the subcortical potential to inhibit cortex. This input is likely
345 responsible for producing the mechanisms of ‘pulsed inhibition’ in the visual cortex [52],
346 reflected by interhemispheric modulation of alpha power, allowing the selective processing
347 of stimuli. Implicitly, we assumed that the volume of the GP indirectly reflects its ability to
348 exert its top-down control over posterior areas, its size possibly representing a determinant
349 for the number of GABAergic neurons involved in the control mechanism.

350 *GP in relation to attentional selection and cognitive control*

351 Interestingly, our results emphasize the specific contribution of the GP in supporting
352 stimulus-driven allocation of attention in a value-based context. The GPi is considered to
353 mediate the output of the BG. Previous literature has implicated this structure in voluntary
354 movement regulation: its functions have indeed been predominantly investigated in clinical
355 and animal models in association with motor functions and action control [12,58], describing,
356 for instance, reduction of hypokinetic and rigidity symptoms following pallidotomy in
357 humans [59,60] and abnormal pallidal activity in monkeys with induced parkinsonism[58].
358 Nevertheless, recent results from single unit recordings in humans have provided indications
359 that electrophysiological activity in the GPi reflects processing of stimuli associated with
360 different reward contingencies [61]. This is corroborated by evidence of alterations of
361 cognitive, in addition to motor, abilities, following pallidotomy in Parkinson's disease
362 patients [62]; In addition, GPi DBS in the treatment of Parkinson's disease has been reported
363 to be associated with several cognitive impairments, such as subtle declines in attention and
364 concentration, although to a lesser extent when compared to subthalamic (STN) DBS [63].
365 This aspect has been further addressed in clinical studies showing a link between Parkinson's
366 disease, associated with abnormal pallidal activity [60,64], and altered reward processing as
367 well as updating [65,66]. Structural GP abnormalities have also been linked to impaired
368 suppression of distractors in ADHD [28,67] as well as psychotic symptoms in schizophrenia
369 [31,33,68], which has been related to aberrant salience attribution and reward learning
370 [34,69]. As an important output component of the reward circuit [70], the GPi might serve to
371 indirectly influence the cortical information flow by biasing selective processing of value-
372 related stimuli. Our data suggest that this influence is further reflected by a modulation of
373 alpha band activity.

374 *Right lateralization of the association between GP and alpha modulation*

375 Interestingly, as visible in Figure 1S, the association between GP lateralization and
376 interhemispheric alpha power was largely related to right hemisphere differences in absolute
377 alpha modulation between subjects exhibiting a right, as compared to left, lateralized GP
378 volume. This finding possibly reflects and is explained by the right hemisphere dominance
379 allegedly characterizing spatial attention processes [71], corroborated by the right lateralized
380 feature of the ventral attentional network, which has been described as specifically involved
381 in the processing of behaviourally salient stimuli [43]

382

383 *Differential role of GP and Th in relation to posterior alpha modulation*

384 Our results show that GP and Th lateralizations were related to the interhemispheric bias in
385 alpha modulation during selective allocation of attention. However, only GP lateralization,
386 and not Th lateralization, was related to the value-saliency pairings in the task. The different
387 contribution from GP and Th in relation to saliency occurrences is likely to reflect different
388 roles of the two networks in the top-down control of attentional processing. The GP provides
389 a modulatory signal related to the processing of stimuli that draw attention due to their strong
390 saliency associations. The perceptual competition resulting from attending to a salient target
391 whilst required to suppress an equally salient distractor, might be resolved by a network
392 involving the GP. Increased midbrain activity has indeed been shown to accompany
393 attentional suppression of a highly rewarding distractor carrying a strong perceptual
394 competition with the target [72], suggesting that dopaminergic networks might flexibly
395 modulate attentional selection in reward-related contexts.

396 The correlation between Th lateralization and attention-related alpha modulation, which was
397 irrespective of the saliency component in the current task, is in line with the notion that
398 thalamic activity, particularly arising from its largest nucleus, the pulvinar, modulates the

399 alpha rhythm in extended visual areas [36,37,73–75]. The pulvinar was first shown to
400 contribute to the generation of the posterior alpha rhythm in dogs [36] and also to regulate
401 synchronized activity between visual cortical areas to support the allocation of attention in
402 human and nonhuman primates [74–77]. Our findings, therefore, add to the growing body of
403 evidence suggesting that thalamo-cortical interactions play a fundamental role in shaping
404 cognitive processing [23,75,78,79]

405

406 *Pallido-cortical pathways*

407 Through which route does the GP influence visual alpha oscillations? A possibility is that the
408 GP modulates prefrontal activity which in turn engages and affects dorsal attentional
409 networks [11,80]. The dorsal attention network, with the intraparietal sulcus (IPS) and frontal
410 eye-fields (FEF) as its major hubs, has been suggested to mediate top-down allocation of
411 attention. Supporting this notion, both the IPS and FEF have been causally implicated in the
412 control over posterior alpha oscillations in relation to attentional shifts [6–8,43,81]. With our
413 results, we propose the existence of a brain network which allows salience driven signals
414 from the BG to influence the prefrontal cortex in biasing the competition among posterior
415 regions. The idea of a BG-cortico loop involved in stimulus driven reorienting of attention
416 has been already introduced [16,82] and is consistent with the notion of a ‘salience network’,
417 which integrates behaviourally relevant input in order to bias and guide cognitive control
418 [83–86]. Within this framework, the BG, through their main output via the GPi, are thought
419 to influence the connectivity between frontoparietal regions by updating goal-directed
420 behaviour, in order to adapt to changes in the environment [87].

421 The influence of GP on posterior alpha oscillations could be mediated through indirect
422 projections via the thalamus. The major target of GPi projections is the motor thalamus,
423 including ventrolateral and ventral anterior thalamic nuclei, which innervates motor and

424 premotor cortex [56,88,89]. However, cortical projections from thalamic nuclei receiving
425 input from the BG might be more diverse and also target prefrontal areas [90], which would
426 enable an indirect modulation of frontoparietal networks by the GPi via the thalamus.
427 Additionally, intra-thalamic connectivity [91,92] as well as complex interactions between the
428 thalamic reticular nucleus and thalamic nuclei [93,94] may provide multiple alternative
429 pathways to convey influence of the GPi on cortical areas and modulate behavior [95]. Note
430 that these pallido-thalamo-cortical pathways are not necessarily related to the volumetric
431 hemispheric lateralization of the thalamus reported here, but might instead represent
432 independent pathways.

433 Another ‘pallido-frontal’ pathway has recently been suggested by Saunders et al. [96],
434 describing specific connections between the external Globus Pallidus (GPe) and prefrontal
435 areas. The authors suggests to extend traditional BG-prefrontal cortex models, by the
436 introduction of a subdivision of GPe cells based on their differential cholinergic marker
437 expression. Employing in vivo extracellular recordings in mice coupled with optogenetics,
438 they demonstrate a direct modulation of frontal cortex by non-cholinergic GPe neurons. Such
439 a projection bypasses canonical BG-cortical networks involving thalamic nuclei. It is
440 interesting to note that the paradigm employed in [96] focused on reward-related behaviour
441 (water reward upon pressure of a lever), hence corroborating our findings relating GP to
442 saliency components of the task. This view is in line with recent evidence in favour of an
443 extension of GPe concept from its well-known ‘relay station’ role within the indirect
444 pathway, to a crucial function in the coordination of neuronal activity in the BG network
445 [97]. On the other hand, attempting to parse specific and exclusive pathways within the BG is
446 likely not the optimal approach given the high level of intra-connectivity patterns within
447 these nuclei [97]. Nevertheless, future investigations might benefit from a more in-depth
448 examination of the role of the subthalamic nucleus in such networks.

449 These proposed models provide a theoretical framework in favor of a flexible subcortical
450 modulation of top-down regulation of attentional allocation, which for the GP appears to be
451 specifically engaged in tasks involving value-saliency processing. Nevertheless, the
452 aforementioned possible modulatory routes should not be considered as mutually exclusive: a
453 more comprehensive model of attentional control should instead account for multiple cortical
454 and subcortical pathways operating in parallel, which would allow optimization of the
455 organism's interaction with the environment.

456

457 **Materials and Methods**

458

459 *Participants*

460 In the present study, we re-analysed the previously acquired dataset described in [38], where
461 twenty-eight healthy volunteers participated in the study (mean age: 23 ± 2.7 years; 17 female;
462 all right handed). All participant reported normal or corrected-to-normal vision and no prior
463 knowledge of Chinese language. Of these, datasets from three participants were excluded
464 from the analysis (due to respectively: technical error during acquisition, excessive eye
465 movements during MEG recording and structural MRI data not acquired), leaving 25
466 participants. The experiment was conducted in compliance with the Declaration of Helsinki
467 and was approved by the local ethics board (CMO region Arnhem-Nijmegen,
468 CMO2001/095).

469

470 *Experimental procedure*

471 The experiment consisted of two phases: in the learning phase, participants were trained to
472 memorize associations between 6 Chinese characters and 3 different values (positive,
473 negative, neutral). Conditioning was implemented by means of visual and auditory feedback:

474 two symbols were associated with reward (+80 cents and a ‘kaching’ sound), two with loss (-
475 80 cents and a ‘buzz’ sound) and two with no value (0 cents and a ‘beep’ sound) (see Figure
476 1A for an example stimulus-reward association). The stimulus-reward pairing was
477 randomized across participants. Each trial started with the display of three fixation crosses
478 (1000ms), followed by the presentation of a Chinese character (1000ms), together with its
479 matching visual and auditory feedback (Figure 1B). Stimuli were displayed on a grey
480 background, each of them was presented twelve times in a randomized order. The learning
481 phase was conducted in a laboratory with attenuated sound and light and without MEG
482 recording. With the aim of reducing extinction, upon completion of this phase participants
483 were informed that the learnt stimulus-feedback associations would be signalling real reward
484 outcomes throughout the testing phase (i.e. the presentation of a Chinese character,
485 irrespective of its role as target or distractor, would result in a financial reward, loss or none).
486 After the learning phase, participants performed a testing phase (Figure 1C), when they were
487 required to perform a covert spatial attention tasks including the stimuli previously associated
488 with a monetary outcome, while ongoing electromagnetic activity was recorded with MEG.
489 In the testing phase, participants performed 8 blocks of 72 trials. Each trial started with the
490 presentation of three fixation crosses for 1000 ms (pre-trial interval), whose contrast
491 subsequently decreased, as a preparatory cue indicating imminent stimuli presentation. After
492 500ms, two symbols were presented to the left and right of the screen (8 degrees visual angle)
493 respectively, together with a central fixation cross flanked by two arrows, indicating the
494 target side. Participants were instructed to covertly attend the symbol on the cued side
495 (‘target’) and to ignore the other one (‘distractor’), until one of them changed contrast. The
496 contrast change either increased or decreased with equal probability, with onset after 750 ms
497 (13% trials), 1450 ms (47% trials, ‘short interval trials’) or 2350 ms (40%, ‘long interval
498 trials’) from stimulus presentation. Participants were asked to report the direction of the

499 contrast change at the targeted ('cued') location as quickly as possible by button press, using
500 the index or middle finger of the right hand to indicate their choice (finger-direction mapping
501 was randomized across participants). Participants were instructed to refrain from responding
502 when the distractor changed contrast. Shorter intervals of 750 ms were used to ensure that
503 participants would start covertly directing their attention rapidly after the cue; these trials
504 were not included in the analysis. The target changed contrast on 95% of the trials (valid
505 trials), whereas in the remaining trials the distractor did (invalid trials). The approximate
506 duration of the full task in the MEG was 50 minutes.

507 As a result of the conditioning manipulation in the learning phase, targets and distractors in
508 the task would be associated with either a salient (positive or negative) or a neutral value,
509 resulting in three categories of trials of interest, as represented by different levels of value-
510 salience, namely: zero (target and distractor neutral), one (target or distractor salient) or two
511 (target and distractor salient) value-salience levels.

512

513 *MEG data acquisition*

514 Electromagnetic brain activity was recorded from participants while seated, using a CTF 275-
515 channels whole-head MEG system with axial gradiometers (CTF MEG Systems, VSM
516 MedTech Ltd.). The data were sampled at 1200Hz, following an antialiasing filter set at
517 300Hz. Head position was constantly monitored throughout the experiment via online head-
518 localization software. This had access to the position of the three head localization coils
519 placed at anatomical fiducials (nasion, left and right ear), allowing, if necessary, readjustment
520 of the participant's position between blocks [98]. Horizontal and vertical EOG and ECG
521 electrodes were recorded with bipolar Ag/AgCl electrodes.

522 *MEG data analysis*

523 MEG data analysis was performed using the FieldTrip Toolbox running in MATLAB [99].
524 Continuous data were segmented in epochs, centred at the onset of the target contrast change,
525 encompassing the preceding 1500 ms and the following 200 ms (this way covering the full
526 stimulus presentation window for short trials). A notch filter was applied at 50, 100, 150 Hz
527 to remove line noise, the mean was subtracted and the linear trend removed. Automatic
528 artifact rejection was implemented for detection and removal of trials containing eye blinks
529 and horizontal eye movements (detected with EOG), MEG sensor jumps and muscle artifacts.
530 We produced virtual planar gradiometers by computing spatial derivatives of the magnetic
531 signal recorded with axial gradiometers [100]. The method has the advantage of improving
532 the interpretation of the topographic mapping since neural sources would produce a gradient
533 field directly above them. Time-frequency representations (TFR) of power were then
534 calculated for the resulting pairs of orthogonal planar gradiometers, before summing the
535 power values at each sensor. The analysis was performed by sliding a fixed time window of
536 500 ms in steps of 50 ms. The resulting data segments were multiplied by a Hanning taper
537 and a fast Fourier transform was applied in the 2 – 30Hz frequency range, in steps of 2Hz.
538 This procedure was applied only for correct valid trials, separately for left and right cued
539 conditions.
540 For each participant, TFRs were averaged across trials and a Modulation Index (MI) was
541 computed for each sensor k and over all time points t belonging to the time window of
542 interest -750 – 0 ms, according to the formula:

$$MI(f)_{k,t} = \frac{Power(f)_{k,t \text{ att right}} - Power(f)_{k,t \text{ att left}}}{Power(f)_{k,t \text{ att right}} + Power(f)_{k,t \text{ att left}}} \quad (1)$$

543 Where $Power(f)_{k,t_{att\ left}}$ represents the power at a given frequency f in the condition
 544 ‘attend left’ and $Power(f)_{k,t_{att\ right}}$ is the power of the same frequency in the condition
 545 ‘attend right’. As a result, positive (or negative) MI values, at a given sensor k and given
 546 timepoint t , indicate higher power at a given frequency f when attention was covertly directed
 547 towards the right (or left) hemifield.

548 Two clusters of sensors were then derived, by selecting the twenty symmetrical occipito-
 549 parietal sensors (i.e. ten pairs of sensors) showing the highest interhemispheric difference in
 550 alpha modulation indices, when considering the grand average over all conditions (see Figure
 551 2A) averaged over the previously defined time window of interest. These clusters constituted
 552 the regions of interests (ROIs) on which subsequent analysis was focused. Subsequently, in
 553 order to quantify individual hemispheric-specific bias with respect to modulation indices in
 554 the alpha range ($MI(\alpha)$), we calculated the Hemispheric Lateralized Modulation (HLM)
 555 index per participant:

$$HLM(\alpha) = \frac{1}{n_{right}} \sum_{k_{right}=1}^{n_{right}} MI(\alpha)_{k_{right}} + \frac{1}{n_{left}} \sum_{k_{left}=1}^{n_{left}} MI(\alpha)_{k_{left}} \quad (2)$$

556 Where k_{left} and k_{right} denote sensors belonging to the aforementioned and previously
 557 defined left and right clusters, respectively. Please note that $MI(\alpha)_k$ indices in Eq.2 (for both
 558 $k=1, \dots, n_{right}$ and $k=1, \dots, n_{left}$) are already a result of an average over timepoints of
 559 interest t . Since $MI(\alpha)$ values were obtained by subtracting alpha power in ‘attend left’ trials
 560 from ‘attend right’ trials, and given that, as a result of attentional allocation, alpha power is
 561 suppressed in the hemisphere contralateral to the attended hemifield, a positive $HLM(\alpha)$

562 value indicated that a given participant displayed higher modulation of absolute magnitude of
563 alpha power in the right compared to the left hemisphere, and vice versa (see Figure 2B).

564 *Structural data acquisition*

565 T1-weighted images of three out of twenty-five participants were acquired on a 3 T MRI
566 scanner (Magnetom TIM Trio, Siemens Healthcare, Erlangen, Germany), acquisition
567 parameters: TR/TE= 2300/3.03 ms; FA=8°; FoV= 256 × 256 mm; slice thickness= 1 mm;
568 Acquisition matrix= 0×256×256×0. For the remaining participants, a 1.5T MRI scanner was
569 used (Magnetom AVANTO, Siemens Healthcare, Erlangen, Germany). Acquisition
570 parameters: TR/TE= 2250/2.95 ms; FA=15°; FoV= 256 × 256 mm; slice thickness= 1 mm;
571 Acquisition matrix= 0×256×256×0.

572

573 *Analysis*

574 Structural analyses were conducted using the Integrated Registration and Segmentation Tool
575 (FIRST) within FMRIB's Software Library (FSL) v5.0.9 (www.fmrib.ox.ac.uk/fsl/, Oxford
576 Centre for Functional MRI of the Brain, Oxford, UK). A standard 12 degrees of freedom
577 affine registration to MNI152 space was applied to individual T1 images, adjusted with
578 optimal sub-cortical weighting. Bayesian models implemented in the software are derived
579 from a training based on previous manual segmentation of 336 datasets (provided by the
580 Center for Morphometric Analysis (CMA, MGH, Boston) and applied to registered images to
581 extract subcortical volumetric outputs for left and right hemispheres (see Figure 3A).
582 Given the reward components of the task we then focused on regions of the basal ganglia
583 identified by the algorithm namely the Globus Pallidus (GP), Nucleus Accumbens (Acb),
584 Caudate (CN), Putamen (Pu), as well as other regions potentially involved in the
585 mechanisms, namely Hippocampus (Hpc), Amygdala (Am) and Thalamus (Th). To compute
586 hemispheric Lateralized Volume indices (LVI) for each substructure of interest s , we used the

587 following formula, which controls for individual differences in specific subcortical volumes
588 via normalization by total bilateral volume, commonly employed to evaluate structural brain
589 asymmetries [34,39]:

$$LV(s) = \frac{V(s)_{right} - V(s)_{left}}{V(s)_{right} + V(s)_{left}} \quad (3)$$

590 Where $V_{S_{right}}$ and $V_{S_{left}}$ represent respectively the anatomical right and left volumes (in
591 voxels) for a given substructure s . Analogously to Eq.(2), a positive (or negative) LV_s index,
592 in a given participant, indicated a greater right (or left) volume for a given substructure s (see
593 Figure 3B).

594 *Statistics*

595 *Generalized Linear Model*

596 In order to determine the relationship between Basal Ganglia Lateralized Volumes (LV_s) and
597 electromagnetic indices ($HLM(\alpha)$) we applied a generalized linear regression model (GLM),
598 specifying subcortical volumes lateralization (LV_s values) as regressors and individual HLM
599 values as the response vector, according to the formula:

$$HLM(\alpha) \sim \beta_0 + \beta_1 LV_{GP} + \beta_2 LV_{NAcc} + \beta_3 LV_{CN} + \beta_4 LV_{Pu} + \beta_5 LV_{HPC} + \beta_6 LV_{Am} + \beta_7 LV_{TH} + \varepsilon \quad (4)$$

600 All subsequent analysis on the relationship between volumetric and oscillatory data
601 specifically focused only on the subcortical structure(s) associated with a significant β
602 coefficient in the model in Eq.(4), below referred as LV_s .

603 *Cluster based permutation test*

604 To evaluate whether the linear association between LV_s and HLM was effectively limited to
605 the alpha band, a cluster based permutation approach [41] was employed over the full time
606 frequency spectrum of interest. This method effectively allows to statistically control for
607 multiple comparisons over all time and frequency points of interest. After selecting the *a-*
608 *priori* sensors belonging to the formerly specified ROIs, we considered a permutation
609 distribution of regression coefficients derived from randomly pairing participants' LV_s value
610 (independent variable) and modulation indices ($HLM(f)$) 1000 times. At every time-by-
611 frequency point, the actual regression coefficient was evaluated against the aforementioned
612 distribution by means of a specified critical α value. Afterwards, a time-frequency map of the
613 cluster level statistics was derived showing sets of sensors associated with a significant
614 effect.

615 An equivalent approach was later applied to investigate possible hemisphere-specific
616 differences in alpha modulation between participants showing a right or left lateralized
617 substructure s . Directionality of lateralization was determined by median split of the
618 distribution of LV_s per participant, producing two subgroups of $N=12$, representing subjects
619 with a larger left or right volume of substructure s . After having a-priori averaged across the
620 time-frequency spectrum of interest ($[-750\ 0]$ ms, 8-13Hz), $MI(\alpha)$ values at every sensor were
621 compared between the two subgroups (right vs left lateralized substructure). The actual t -
622 value was then compared with a permutation distribution of t -statistic derived from randomly
623 partitioning indices between the two groups 1000 times. As a result, a topography map was
624 plotted displaying eventual cluster(s) of sensors associated with a significant t -value (i.e. a
625 significant difference in $MI(\alpha)$ between subgroups).

626 *Comparison between Pearson's correlation coefficients*

627 Finally, we aimed at comparing the association between the derived structural and functional
628 lateralization indices in different value salience occurrences. To this end, we calculated
629 HLM(α) values for each participant separately for the three reward-related contingencies and
630 computed the Pearson's correlations with LV_S indices which displayed a significant β as
631 arising from the model in Eq.(4). We statistically assessed the difference in correlation
632 coefficients between the three experimental conditions considered, according to the method
633 described in [101]. The test implements a percentile resampling technique by generating a
634 bootstrap sample of the difference of the correlation coefficients between the overlapping
635 variable LV_{GP}(Y) and the two variables representing the HLM(α) for the two experimental
636 conditions (VO levels) to be compared (X_1, X_2). As suggested in the method, we used a
637 Winsorized correlation to achieve a robust measure of association between variables. This
638 transformation has been shown to effectively control for the influence of outliers on the
639 correlation estimate [102]. A confidence interval was then computed on the resulting
640 bootstrap distribution, to assess the statistical significance of the actual difference between
641 correlation coefficients describing the different VOs.

642

643 *Behavioural data analysis*

644 To assess whether subjects displayed a spatial bias during the task, we first averaged across
645 left and right cued trials separately, averaged across all conditions (i.e., irrespective of value-
646 saliency occurrences (VO)). We then employed paired t-test on the derived reaction times
647 (RT) and accuracy (ACC) (expressed as percentage of correct responses) measures for the
648 left and right cued trials. Secondly, we divided trials according to VO pairings, averaging left
649 and right cued trials, to determine whether behavioural performance varied as a function of
650 saliency in both RT and ACC. We here employed one-way repeated measures ANOVA to

651 assess whether group means in the three conditions significantly differ from each other. We
652 also considered individual lateralized measures of RT and ACC across different VO
653 conditions. To this end, behavioural asymmetries in performance (BA) for both measures
654 were calculated according to:

$$BA_{RT/ACC} = \frac{BA_{RT/ACC_{right}} - BA_{RT/ACC_{left}}}{BA_{RT/ACC_{right}} + BA_{RT/ACC_{left}}} \quad (5)$$

655 Where $BA_{RT_{right}}$ and $BA_{RT_{left}}$ represent mean reaction times for 'attend right' and 'attend left'
656 trials, respectively. A positive BA_{RT} for a given subject indicated faster responses when a
657 participant was validly cued to the left compared to the right hemisphere, while negative
658 values indicated the opposite pattern. Consequently, positive BA_{ACC} values indicated higher
659 accuracy on 'attend right' trials compared to 'left attend' trials, and vice versa.

660 A one-way repeated measures ANOVA was employed to test the difference across group
661 means in the three VO conditions examined.

662 In a next step, we sought to investigate the possible association of behavioural performance
663 with structural and functional hemispheric lateralization, we used Pearson's correlation to
664 examine the association of individual asymmetries in accuracy (BA_{ACC}) and reaction times
665 (BA_{RT}) with individual $HLM(\alpha)$ and LV values of subcortical structures which showed
666 significant correlation with $HLM(\alpha)$.

667 In a last step, we employed a general linear model (GLM) in order to assess whether spatial
668 biases in behavioural performance could be explained by a combination of the other
669 variables, namely $HLM(\alpha)$ and the LV indices of the subcortical areas considered, according
670 to the formula:

$$BA_{RT/ACC} \sim \beta_0 + \beta_1 LV_{GP} + \beta_2 LV_{NAcc} + \beta_3 LV_{CN} + \beta_4 LV_{Pu} + \beta_5 LV_{HPC} + \beta_6 LV_{Am} + \beta_7 LV_{TH} + \beta_4 HLM(\alpha) + \varepsilon \quad (6)$$

671 *Data availability*

672 The preprocessed MEG and MRI anonymised datasets that support the findings of this study
673 are available as downloadable online data collection in the Donders Data Repository
674 (<https://data.donders.ru.nl>), with persistent identifier: [11633/di.dccn.DSC_3016045.01_337](https://doi.org/10.11633/di.dccn.DSC_3016045.01_337),
675 upon reasonable request to the corresponding author.

676

677 **Acknowledgements**

678 The authors gratefully acknowledge the support of the Netherlands Organisation for
679 Scientific Research (NWO, VICI grants 453-09-002 and 453-14-015 and the James S.
680 McDonnell Foundation (grants 220020328 and 220020448). We also would like to thank
681 Sebastiaan den Boer for his contribution in the data collection process and experimental
682 design.

683 **References**

- 684 1. Nobre, K., & Kastner S. The Oxford handbook of attention. Oxford: Oxford University
685 Press; 2014.
- 686 2. Chelazzi L, Perlato A, Santandrea E, Della Libera C. Rewards teach visual selective
687 attention. *Vision Res.* Elsevier Ltd; 2013;85: 58–62. doi:10.1016/j.visres.2012.12.005
- 688 3. Thut G. -Band Electroencephalographic Activity over Occipital Cortex Indexes
689 Visuospatial Attention Bias and Predicts Visual Target Detection. *J Neurosci.* 2006;26:
690 9494–9502. doi:10.1523/JNEUROSCI.0875-06.2006
- 691 4. Kelly SP. Increases in Alpha Oscillatory Power Reflect an Active Retinotopic
692 Mechanism for Distracter Suppression During Sustained Visuospatial Attention. *J*
693 *Neurophysiol.* 2006;95: 3844–3851. doi:10.1152/jn.01234.2005
- 694 5. Worden MS, Foxe JJ, Wang N, Simpson G V. Anticipatory biasing of visuospatial
695 attention indexed by retinotopically specific alpha-band electroencephalography
696 increases over occipital cortex. *J Neurosci.* 2000;20: RC63.
- 697 6. Ptak R. The Frontoparietal Attention Network of the Human Brain. *Neurosci.* 2012;18:
698 502–515. doi:10.1177/1073858411409051
- 699 7. Vossel S, Geng JJ, Fink GR. Dorsal and Ventral Attention Systems. *Neurosci.*
700 2014;20: 150–159. doi:10.1177/1073858413494269
- 701 8. Marshall TR, Bergmann TO, Jensen O. Frontoparietal Structural Connectivity
702 Mediates the Top-Down Control of Neuronal Synchronization Associated with
703 Selective Attention. *PLoS Biol.* 2015;13: 1–17. doi:10.1371/journal.pbio.1002272
- 704 9. Marshall TR, O’Shea J, Jensen O, Bergmann TO. Frontal Eye Fields Control
705 Attentional Modulation of Alpha and Gamma Oscillations in Contralateral
706 Occipitoparietal Cortex. *J Neurosci.* 2015;35: 1638–1647.

- 707 doi:10.1523/JNEUROSCI.3116-14.2015
- 708 10. Capotosto P, Corbetta M, Romani GL, Babiloni C. Electrophysiological correlates of
709 stimulus-driven reorienting deficits after interference with right parietal cortex during
710 a spatial attention task: a TMS-EEG study. *J Cogn Neurosci*. 2012;24:
711 10.1162/jocn_a_00287. doi:10.1162/jocn_a_00287
- 712 11. Cummings J. Frontal-subcortical circuits and human behavior. *Arch Neurol*. 1993;50:
713 873–880. doi:10.1001/archneur.1993.00540080076020
- 714 12. Jahfari S, Waldorp L, van den Wildenberg WPM, Scholte HS, Ridderinkhof KR,
715 Forstmann BU. Effective Connectivity Reveals Important Roles for Both the
716 Hyperdirect (Fronto-Subthalamic) and the Indirect (Fronto-Striatal-Pallidal) Fronto-
717 Basal Ganglia Pathways during Response Inhibition. *J Neurosci*. 2011;31: 6891–6899.
718 doi:10.1523/JNEUROSCI.5253-10.2011
- 719 13. Braunlich K, Seger C. The basal ganglia. *Wiley Interdiscip Rev Cogn Sci*. 2013;4:
720 135–148. doi:10.1002/wcs.1217
- 721 14. Tomer R, Goldstein RZ, Wang G-J, Wong C, Volkow ND. Incentive motivation is
722 associated with striatal dopamine asymmetry. *Biol Psychol*. 2008;77: 98–101.
723 doi:10.1016/j.biopsycho.2007.08.001
- 724 15. Tomer R, Slagter HA, Christian BT, Fox AS, King CR, Murali D, et al. Dopamine
725 Asymmetries Predict Orienting Bias in Healthy Individuals. *Cereb Cortex*. 2013;23:
726 2899–2904. doi:10.1093/cercor/bhs277
- 727 16. Shulman GL, Astafiev S V, Franke D, Pope DLW, Abraham Z, Mcavoy MP, et al.
728 Interaction of stimulus-driven reorienting and expectation in ventral and dorsal fronto-
729 parietal and basal ganglia-cortical networks. 2010;29: 4392–4407.
730 doi:10.1523/JNEUROSCI.5609-08.2009.Interaction

- 731 17. Hikosaka O, Bromberg-Martin E, Hong S, Matsumoto M. New insights on the
732 subcortical representation of reward. *Curr Opin Neurobiol.* 2008;18: 203–208.
733 doi:10.1016/j.conb.2008.07.002
- 734 18. Hikosaka O, Kim HF, Yasuda M, Yamamoto S. Basal Ganglia Circuits for Reward
735 Value–Guided Behavior. *Annu Rev Neurosci.* 2014;37: 289–306.
736 doi:10.1146/annurev-neuro-071013-013924
- 737 19. Schechtman E, Noblejas MI, Mizrahi AD, Dauber O, Bergman H. Pallidal spiking
738 activity reflects learning dynamics and predicts performance. *Proc Natl Acad Sci.*
739 2016;113: E6281–E6289. doi:10.1073/pnas.1612392113
- 740 20. Lauwereyns J, Takikawa Y, Kawagoe R, Kobayashi S, Koizumi M, Coe B, et al.
741 Feature-based anticipation of cues that predict reward in monkey caudate nucleus.
742 *Neuron.* 2002;33: 463–473. doi:10.1016/S0896-6273(02)00571-8
- 743 21. Schultz W, Tremblay L, Hollerman JR, Schultz. Reward processing in primate
744 orbitofrontal cortex and basal ganglia. *Cereb Cortex.* 2000;10: 272–284.
745 doi:10.1093/cercor/10.3.272
- 746 22. Tremblay L, Hollerman JR, Schultz W. Modifications of reward expectation-related
747 neuronal activity during learning in primate striatum. *J Neurophysiol.* 1998;80: 964–
748 977.
- 749 23. Saalman YB, Kastner S. Cognitive and Perceptual Functions of the Visual Thalamus.
750 *Neuron.* Elsevier Inc.; 2011;71: 209–223. doi:10.1016/j.neuron.2011.06.027
- 751 24. Shipp S. The brain circuitry of attention. *Trends Cogn Sci.* 2004;8: 223–230.
752 doi:10.1016/j.tics.2004.03.004
- 753 25. van Schouwenburg M, Aarts E, Cools R. Dopaminergic modulation of cognitive
754 control: distinct roles for the prefrontal cortex and the basal ganglia. *Curr Pharm Des.*

- 755 2010;16: 2026–2032. doi:10.2174/138161210791293097
- 756 26. Van Schouwenburg MR, Den Ouden HEM, Cools R. Selective attentional
757 enhancement and inhibition of fronto-posterior connectivity by the basal ganglia
758 during attention switching. *Cereb Cortex*. 2015;25: 1527–1534.
759 doi:10.1093/cercor/bht345
- 760 27. Tommasi G, Fiorio M, Yelnik J, Krack P, Sala F, Schmitt E, et al. Disentangling the
761 Role of Cortico-Basal Ganglia Loops in Top–Down and Bottom–Up Visual Attention:
762 An Investigation of Attention Deficits in Parkinson Disease. *J Cogn Neurosci*. MIT
763 Press; 2014;27: 1215–1237. doi:10.1162/jocn_a_00770
- 764 28. Aylward EH, Reiss AL, Reader MJ, Singer HS, Brown JE, Denckla MB. Basal ganglia
765 volumes in children with attention-deficit hyperactivity disorder. *J Child Neurol*.
766 1996;11: 112–115. doi:10.1177/088307389601100210
- 767 29. Qui A, Crocetti D, Adler M, Mahone EM, Denckla MB, Miller MI, et al. Basal ganglia
768 volume and shape in children with attention deficit hyperactivity disorder. *Am J*
769 *Psychiatry*. 2009;166: 74–82. doi:10.1176/appi.ajp.2008.08030426.Basal
- 770 30. Paclt I, Přibilová N, Kollárová P, Kohoutová M, Dezortová M, Hájek M, et al. Reverse
771 asymmetry and changes in brain structural volume of the basal ganglia in ADHD,
772 developmental changes and the impact of stimulant medications. *Neuroendocrinol*
773 *Lett*. 2016;37: 29–32.
- 774 31. Hokama H, Shenton ME, Nestor PG, Kikinis R, Levitt JJ, Metcalf D, et al. Caudate,
775 putamen, and globus pallidus volume in schizophrenia: A quantitative MRI study.
776 *Psychiatry Res Neuroimaging*. 1995;61: 209–229. doi:10.1016/0925-4927(95)02729-
777 H
- 778 32. Womer FY, Wang L, Alpert KI, Smith MJ, Csernansky JG, Barch DM, et al. Basal

- 779 ganglia and thalamic morphology in schizophrenia and bipolar disorder. *Psychiatry*
780 *Res - Neuroimaging*. Elsevier; 2014;223: 75–83.
781 doi:10.1016/j.psychresns.2014.05.017
- 782 33. Mamah D, Wang L, Barch D, de Erausquin GA, Gado M, Csernansky JG. Structural
783 analysis of the basal ganglia in schizophrenia. *Schizophr Res*. 2007;89: 59–71.
784 doi:10.1016/j.schres.2006.08.031
- 785 34. Okada N, Fukunaga M, Yamashita F, Koshiyama D, Yamamori H, Ohi K, et al.
786 Abnormal asymmetries in subcortical brain volume in schizophrenia. *Mol Psychiatry*.
787 Nature Publishing Group; 2016;21: 1–7. doi:10.1038/mp.2015.209
- 788 35. Howes OD, Nour MM. Dopamine and the aberrant salience hypothesis of
789 schizophrenia. *World Psychiatry*. 2016;15: 3–4. doi:10.1002/wps.20276
- 790 36. Lopes da Silva FH, Vos JE, Mooibroek J, van Rotterdam A. Relative contributions of
791 intracortical and thalamo-cortical processes in the generation of alpha rhythms,
792 revealed by partial coherence analysis. *Electroencephalogr Clin Neurophysiol*.
793 1980;50: 449–456. doi:10.1016/0013-4694(80)90011-5
- 794 37. Zhou H, Schafer RJ, Desimone R. Pulvinar-Cortex Interactions in Vision and
795 Attention. *Neuron*. Elsevier Inc.; 2016;89: 209–220. doi:10.1016/j.neuron.2015.11.034
- 796 38. Marshall TR, den Boer S, Cools R, Jensen O, Fallon SJ, Zumer JM. Occipital Alpha
797 and Gamma Oscillations Support Complementary Mechanisms for Processing
798 Stimulus Value Associations. *J Cogn Neurosci*. MIT Press; 2017; 1–11.
799 doi:10.1162/jocn_a_01185
- 800 39. Guadalupe T, Mathias SR, VanErp TGM, Whelan CD, Zwiers MP, Abe Y, et al.
801 Human subcortical brain asymmetries in 15,847 people worldwide reveal effects of
802 age and sex. *Brain Imaging Behav*. 2016; 1–18. doi:10.1007/s11682-016-9629-z

- 803 40. Dillon DG, Holmes AJ, Birk JL, Brooks N, Lyons-Ruth K, Pizzagalli DA. Childhood
804 Adversity Is Associated with Left Basal Ganglia Dysfunction During Reward
805 Anticipation in Adulthood. *Biol Psychiatry. Society of Biological Psychiatry*; 2009;66:
806 206–213. doi:10.1016/j.biopsych.2009.02.019
- 807 41. Maris E, Oostenveld R. Nonparametric statistical testing of EEG- and MEG-data. *J*
808 *Neurosci Methods*. 2007;164: 177–190. doi:10.1016/j.jneumeth.2007.03.024
- 809 42. Wilcox RR. Comparing dependent robust correlations. *Br J Math Stat Psychol*.
810 2016;69: 215–224. doi:10.1111/bmsp.12069
- 811 43. Corbetta M, Shulman GL. Control of Goal-Directed and Stimulus-Driven Attention in
812 the Brain. *Nat Rev Neurosci*. 2002;3: 215–229. doi:10.1038/nrn755
- 813 44. Marshall TR, O’Shea J, Jensen O, Bergmann TO. Frontal Eye Fields Control
814 Attentional Modulation of Alpha and Gamma Oscillations in Contralateral
815 Occipitoparietal Cortex. *J Neurosci*. 2015;35: 1638–1647.
816 doi:10.1523/JNEUROSCI.3116-14.2015
- 817 45. Slagter HA, Mazaheri A, Reteig LC, Smolders R, Figeer M, Mantione M, et al.
818 Contributions of the ventral striatum to conscious perception: An intracranial EEG
819 study of the attentional blink. *J Neurosci*. 2016;37: 1081–1089.
820 doi:10.1523/JNEUROSCI.2282-16.2016
- 821 46. Frank MJ, Loughry B, O’Reilly RC. Interactions between frontal cortex and basal
822 ganglia in working memory: A computational model. *Cogn Affect Behav Neurosci*.
823 2001;1: 137–160. doi:10.3758/CABN.1.2.137
- 824 47. Reilly RCO, Herd SA, Pauli WM. Computational Models of Cognitive Control.
825 *Psychology*. 2011;20: 257–261. doi:10.1016/j.conb.2010.01.008.Computational
- 826 48. Ceaser AE, Barch DM. Striatal Activity is Associated with Deficits of Cognitive

- 827 Control and Aberrant Salience for Patients with Schizophrenia. *Front Hum Neurosci.*
828 2015;9: 687. doi:10.3389/fnhum.2015.00687
- 829 49. Piray P, Toni I, Cools R. Human Choice Strategy Varies with Anatomical Projections
830 from Ventromedial Prefrontal Cortex to Medial Striatum. *J Neurosci.* 2016;36: 2857–
831 2867. doi:10.1523/JNEUROSCI.2033-15.2016
- 832 50. Yantis S, Anderson BA, Wampler EK, Laurent PA. Reward and attentional control in
833 visual search. *Nebr Symp Motiv.* 2012;59: 91–116. doi:10.1111/j.1600-
834 6143.2008.02497.x.Plasma
- 835 51. Tommasi G, Fiorio M, Yelnik J, Krack P, Sala F, Schmitt E, et al. Disentangling the
836 Role of Cortico-Basal Ganglia Loops in Top–Down and Bottom–Up Visual Attention:
837 An Investigation of Attention Deficits in Parkinson Disease. *J Cogn Neurosci.* MIT
838 Press; 2015;27: 1215–1237. doi:10.1162/jocn_a_00770
- 839 52. Jensen O, Mazaheri A. Shaping functional architecture by oscillatory alpha activity:
840 gating by inhibition. *Front Hum Neurosci.* 2010;4: 186.
841 doi:10.3389/fnhum.2010.00186
- 842 53. Fries P. Modulation of Oscillatory Neuronal Synchronization by Selective Visual
843 Attention. *Science (80-).* 2001;291: 1560–1563. doi:10.1126/science.1055465
- 844 54. Fallon SJ, Zokaei N, Norbury A, Manohar SG, Husain M. Dopamine Alters the
845 Fidelity of Working Memory Representations according to Attentional Demands. *J*
846 *Cogn Neurosci.* 2017;29: 728–738. doi:10.1162/jocn_a_01073
- 847 55. Fallon SJ, Cools R. Reward acts on the pFC to enhance distractor resistance of
848 working memory representations. *J Cogn Neurosci.* MIT Press; 2014;26: 2812–2826.
- 849 56. Goldberg JH, Farries MA, Fee MS. Basal ganglia output to the thalamus: still a
850 paradox. *Trends Neurosci.* 2013;36: 10.1016/j.tins.2013.09.001.

- 851 doi:10.1016/j.tins.2013.09.001
- 852 57. Lanciego JL, Luquin N, Obeso JA. Functional neuroanatomy of the basal ganglia.
853 Cold Spring Harb Perspect Med. 2012;2: 1–20. doi:10.1101/cshperspect.a009621
- 854 58. Filion M, Tremblay L. Abnormal spontaneous activity of globus pallidus neurons in
855 monkeys with MPTP-induced parkinsonism. Brain Res. 1991;547: 140–144.
856 doi:10.1016/0006-8993(91)90585-J
- 857 59. Schuurman PR, de Bie RMA, Speelman JD, Bosch DA. Posteroventral Pallidotomy in
858 Movement Disorders. In: Ostertag CB, Thomas DGT, Bosch A, Linderoth B, Broggi
859 G, editors. Advances in Stereotactic and Functional Neurosurgery 12: Proceedings of
860 the 12th Meeting of the European Society for Stereotactic and Functional
861 Neurosurgery, Milan 1996. Vienna: Springer Vienna; 1997. pp. 14–17.
862 doi:10.1007/978-3-7091-6513-3_3
- 863 60. Dostrovsky JO, Hutchison WD, Lozano AM. The Globus Pallidus , Deep Brain
864 Stimulation , and Parkinson ’ s Disease. Neurosci. 2002;8: 284–290.
865 doi:10.1177/1073858402008003014
- 866 61. Howell NA, Prescott IA, Lozano AM, Hodaie M, Voon V, Hutchison WD.
867 Preliminary evidence for human globus pallidus pars interna neurons signaling reward
868 and sensory stimuli. Neuroscience. IBRO; 2016;328: 30–39.
869 doi:10.1016/j.neuroscience.2016.04.020
- 870 62. Lombardi WJ, Gross RE, Trepanier LL, Lang AE, Lozano AM, Saint-Cyr JA.
871 Relationship of lesion location to cognitive outcome following microelectrode-guided
872 pallidotomy for Parkinson’s disease: support for the existence of cognitive circuits in
873 the human pallidum. Brain. 2000;123: 746–758. doi:10.1093/brain/123.4.746
- 874 63. Combs HL, Folley BS, Berry DTR, Segerstrom SC, Han DY, Anderson-Mooney AJ,

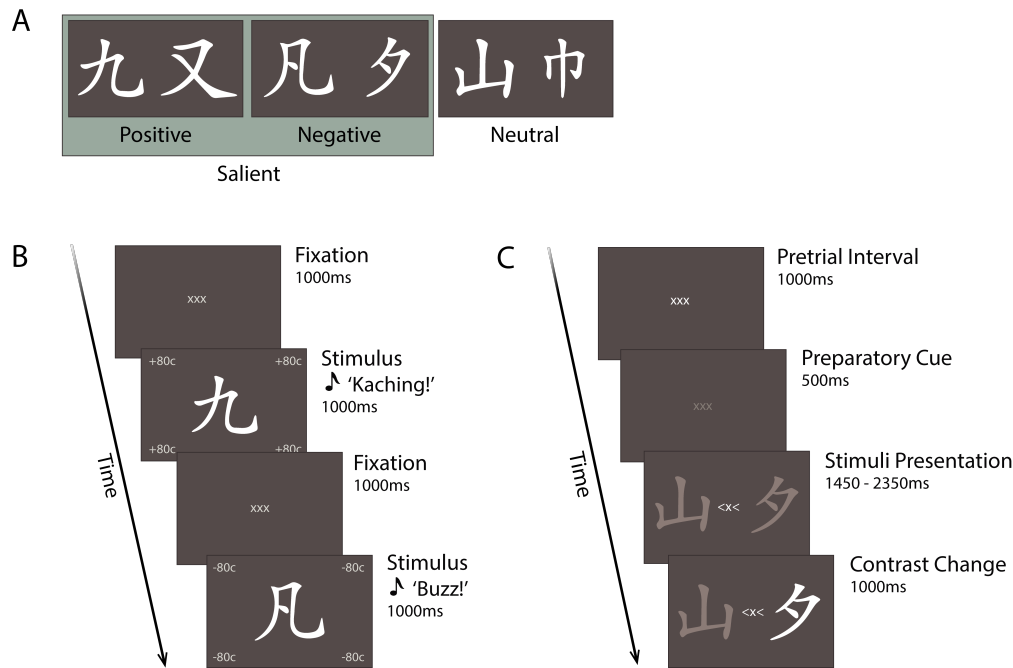
- 875 et al. Cognition and Depression Following Deep Brain Stimulation of the Subthalamic
876 Nucleus and Globus Pallidus Pars Internus in Parkinson's Disease: A Meta-Analysis.
877 *Neuropsychol Rev.* 2015;25: 439–454. doi:10.1007/s11065-015-9302-0
- 878 64. Rosenberg-Katz K, Herman T, Jacob Y, Kliper E, Giladi N, Hausdorff JM. Subcortical
879 Volumes Differ in Parkinson's Disease Motor Subtypes: New Insights into the
880 Pathophysiology of Disparate Symptoms. *Front Hum Neurosci.* 2016;10: 1–9.
881 doi:10.3389/fnhum.2016.00356
- 882 65. Aarts E, Helmich RC, Janssen MJR, Oyen WJG, Bloem BR, Cools R. Aberrant reward
883 processing in Parkinson's disease is associated with dopamine cell loss. *Neuroimage.*
884 Elsevier Inc.; 2012;59: 3339–3346. doi:10.1016/j.neuroimage.2011.11.073
- 885 66. Chong TTJ, Bonnelle V, Manohar S, Veromann KR, Muhammed K, Tofaris GK, et al.
886 Dopamine enhances willingness to exert effort for reward in Parkinson's disease.
887 *Cortex.* Elsevier Ltd; 2015;69: 40–46. doi:10.1016/j.cortex.2015.04.003
- 888 67. Qiu A, Crocetti D, Adler M, Mahone EM, Denckla MB, Miller MI, et al. Basal ganglia
889 volume and shape in children with attention deficit hyperactivity disorder. *Am J*
890 *Psychiatry.* 2009;166: 74–82. doi:10.1176/appi.ajp.2008.08030426
- 891 68. Spinks R, Nopoulos P, Ward J, Fuller R, Magnotta VA, Andreasen NC. Globus
892 pallidus volume is related to symptom severity in neuroleptic naive patients with
893 schizophrenia. *Schizophr Res.* 2005;73: 229–233. doi:10.1016/j.schres.2004.05.020
- 894 69. Early TS, Reiman EM, Raichle ME, Spitznagel EL. Left globus pallidus abnormality
895 in never-medicated patients with schizophrenia. *Proc Natl Acad Sci U S A.* 1987;84:
896 561–563.
- 897 70. Haber S. Neuroanatomy of Reward: A View from the Ventral Striatum. In: Jay A.
898 Gottfried, editor. *Neurobiology of Sensation and Reward.* CRC Press; 2011.

- 899 doi:10.1201/b10776-15
- 900 71. Shulman GL, Pope DLW, Astafiev S V., McAvoy MP, Snyder AZ, Corbetta M. Right
901 Hemisphere Dominance during Spatial Selective Attention and Target Detection
902 Occurs Outside the Dorsal Frontoparietal Network. *J Neurosci.* 2010;30: 3640–3651.
903 doi:10.1523/JNEUROSCI.4085-09.2010
- 904 72. Gong M, Jia K, Li S. Perceptual Competition Promotes Suppression of Reward
905 Salience in Behavioral Selection and Neural Representation. *J Neurosci.* 2017;37:
906 6242–6252. doi:10.1523/JNEUROSCI.0217-17.2017
- 907 73. Wilke M, Mueller K-M, Leopold DA. Neural activity in the visual thalamus reflects
908 perceptual suppression. *Proc Natl Acad Sci.* 2009;106: 9465–9470.
909 doi:10.1073/pnas.0900714106
- 910 74. Saalmann YB, Pinsk MA, Wang L, Li X, Kastner S. The Pulvinar Regulates
911 Information Transmission Between Cortical Areas Based on Attention Demands.
912 *Science* (80-). 2012;337: 753–756. doi:10.1126/science.1223082
- 913 75. Green JJ, Boehler CN, Roberts KC, Chen L-C, Krebs RM, Song AW, et al. Cortical
914 and Subcortical Coordination of Visual Spatial Attention Revealed by Simultaneous
915 EEG–fMRI Recording. *J Neurosci.* 2017;37: 7803–7810.
916 doi:10.1523/JNEUROSCI.0326-17.2017
- 917 76. Petersen SE, Robinson DL, Morris JD. Contributions of the pulvinar to visual spatial
918 attention. *Neuropsychologia.* 1987;25: 97–105. doi:10.1016/0028-3932(87)90046-7
- 919 77. Kastner S, O’Connor DH, Fukui MM, Fehd HM, Herwig U, Pinsk MA. Functional
920 imaging of the human lateral geniculate nucleus and pulvinar. *J Neurophysiol.*
921 2004;91: 438–448. doi:10.1152/jn.00553.2003
- 922 78. Halassa MM, Kastner S. Thalamic functions in distributed cognitive control. *Nat*

- 923 Neurosci. Springer US; 2017;20: 1669–1679. doi:10.1038/s41593-017-0020-1
- 924 79. Sherman SM. Thalamus plays a central role in ongoing cortical functioning. Nat
925 Neurosci. 2016;19: 533–541. doi:10.1038/nn.4269
- 926 80. Pauls DL, Abramovitch A, Rauch SL, Geller DA. Obsessive–compulsive disorder: an
927 integrative genetic and neurobiological perspective. Nat Rev Neurosci. Nature
928 Publishing Group; 2014;15: 410–424. doi:10.1038/nrn3746
- 929 81. Capotosto P, Corbetta M, Romani GL, Babiloni C. Electrophysiological correlates of
930 stimulus-driven reorienting deficits after interference with right parietal cortex during
931 a spatial attention task: a TMS-EEG study. J Cogn Neurosci. 2012;24:
932 10.1162/jocn_a_00287. doi:10.1162/jocn_a_00287
- 933 82. Alexander G. Parallel Organization of Functionally Segregated Circuits Linking Basal
934 Ganglia and Cortex. Annu Rev Neurosci. 1986;9: 357–381.
935 doi:10.1146/annurev.neuro.9.1.357
- 936 83. Metzger CD. High field fMRI reveals thalamocortical integration of segregated
937 cognitive and emotional processing in mediodorsal and intralaminar thalamic nuclei.
938 Front Neuroanat. 2010;4: 1–17. doi:10.3389/fnana.2010.00138
- 939 84. Peters SK, Dunlop K, Downar J. Cortico-Striatal-Thalamic Loop Circuits of the
940 Salience Network: A Central Pathway in Psychiatric Disease and Treatment. Front
941 Syst Neurosci. 2016;10: 1–23. doi:10.3389/fnsys.2016.00104
- 942 85. Seeley WW, Menon V, Schatzberg AF, Keller J, Glover GH, Kenna H, et al.
943 Dissociable Intrinsic Connectivity Networks for Salience Processing and Executive
944 Control. J Neurosci. 2007;27: 2349–2356. doi:10.1523/JNEUROSCI.5587-06.2007
- 945 86. Chen MC, Ferrari L, Sacchet MD, Foland-Ross LC, Qiu MH, Gotlib IH, et al.
946 Identification of a direct GABAergic pallidocortical pathway in rodents. Eur J

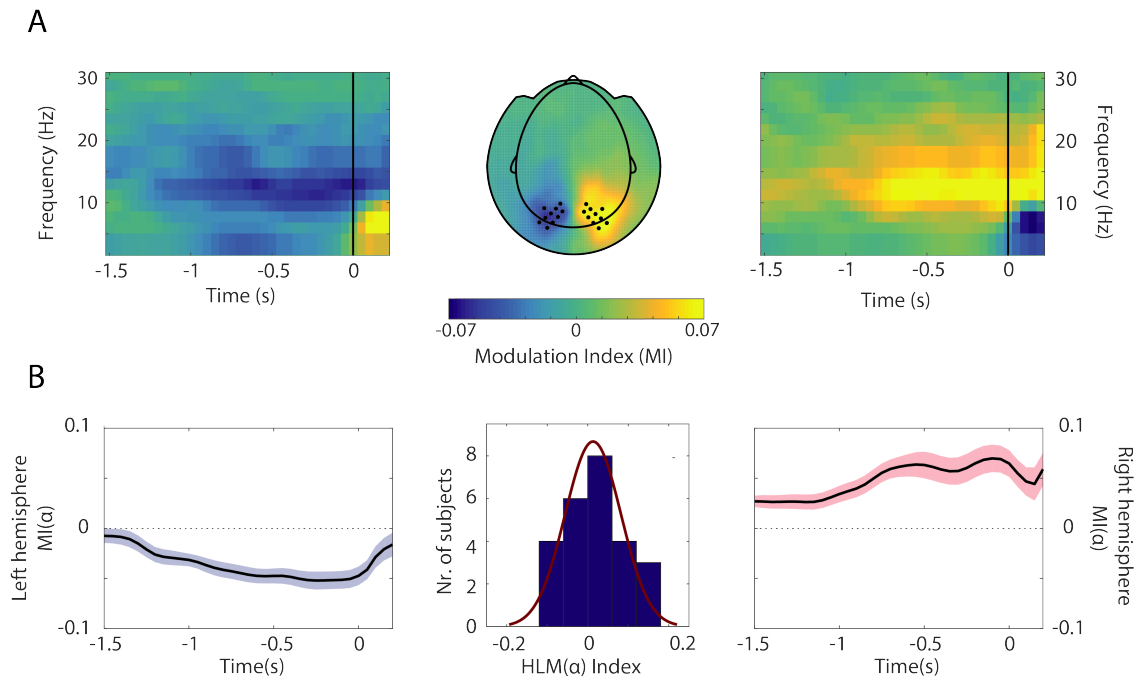
- 947 Neurosci. 2015;41: 748–759. doi:10.1111/ejn.12822
- 948 87. van Schouwenburg MR, den Ouden HEM, Cools R. The Human Basal Ganglia
949 Modulate Frontal-Posterior Connectivity during Attention Shifting. J Neurosci.
950 2010;30: 9910–9918. doi:10.1523/JNEUROSCI.1111-10.2010
- 951 88. Herrero MT, Barcia C, Navarro JM. Functional anatomy of thalamus and basal
952 ganglia. Child’s Nerv Syst. 2002;18: 386–404. doi:10.1007/s00381-002-0604-1
- 953 89. Sommer MA. The role of the thalamus in motor control. Curr Opin Neurobiol.
954 2003;13: 663–670. doi:10.1016/j.conb.2003.10.014
- 955 90. McFarland NR, Haber SN. Thalamic relay nuclei of the basal ganglia form both
956 reciprocal and nonreciprocal cortical connections, linking multiple frontal cortical
957 areas. J Neurosci. 2002;22: 8117–32. doi:22/18/8117 [pii]
- 958 91. Crabtree JW, Isaac JTR. New intrathalamic pathways allowing modality-related and
959 cross-modality switching in the dorsal thalamus. J Neurosci. 2002;22: 8754–8761.
960 doi:22/19/8754 [pii]
- 961 92. Crabtree JW, Collingridge GL, Isaac JTR. A new intrathalamic pathway linking
962 modality-related nuclei in the dorsal thalamus. Nat Neurosci. 1998;1: 389–394.
963 doi:10.1038/1603
- 964 93. Guillery RW, Feig SL, Lozsádi D a., Lozsadi DA, Lozsádi D a. Paying attention to the
965 thalamic reticular nucleus. Trends Neurosci. 1998;21: 28–32. doi:10.1016/S0166-
966 2236(97)01157-0
- 967 94. Halassa MM, Acsády L. Thalamic Inhibition: Diverse Sources, Diverse Scales. Trends
968 Neurosci. Elsevier Ltd; 2016;39: 680–693. doi:10.1016/j.tins.2016.08.001
- 969 95. Haber SN, Calzavara R. The cortico-basal ganglia integrative network: The role of the
970 thalamus. Brain Res Bull. 2009;78: 69–74. doi:10.1016/j.brainresbull.2008.09.013

- 971 96. Saunders A, Oldenburg IA, Berezovskii VK, Johnson CA, Kingery ND, Elliott HL, et
972 al. A direct GABAergic output from the basal ganglia to frontal cortex. *Nature*.
973 2015;521: 85–89. doi:10.1038/nature14179
- 974 97. Deffains M, Iskhakova L, Bergman H. Stop and Think about Basal Ganglia Functional
975 Organization: The Pallido-Striatal “Stop” Route. *Neuron*. 2016;89: 237–239.
976 doi:10.1016/j.neuron.2016.01.003
- 977 98. Stolk A, Todorovic A, Schoffelen JM, Oostenveld R. Online and offline tools for head
978 movement compensation in MEG. *Neuroimage*. Elsevier Inc.; 2013;68: 39–48.
979 doi:10.1016/j.neuroimage.2012.11.047
- 980 99. Oostenveld R, Fries P, Maris E, Schoffelen JM. FieldTrip: Open source software for
981 advanced analysis of MEG, EEG, and invasive electrophysiological data. *Comput*
982 *Intell Neurosci*. 2011;2011. doi:10.1155/2011/156869
- 983 100. Bastiaansen MCM, Knösche TR. Tangential derivative mapping of axial MEG applied
984 to event-related desynchronization research. *Clin Neurophysiol*. 2000;111: 1300–1305.
985 doi:10.1016/S1388-2457(00)00272-8
- 986 101. Wilcox RR. Comparing dependent robust correlations. *Br J Math Stat Psychol*.
987 2016;69: 215–224. doi:10.1111/bmsp.12069
- 988 102. Wilcox RR. *Introduction to Robust Estimation and Hypothesis Testing*. Academic
989 Press; 2016.
- 990 103. Bischoff-Grethe A, Ozyurt IB, Busa E, Quinn BT, Fennema-Notestine C, Clark CP, et
991 al. A technique for the deidentification of structural brain MR images. *Hum Brain*
992 *Mapp*. 2007;28: 892–903. doi:10.1002/hbm.20312



993 **Figure 1. Illustration of selective attention task: stimuli and reward manipulation.**

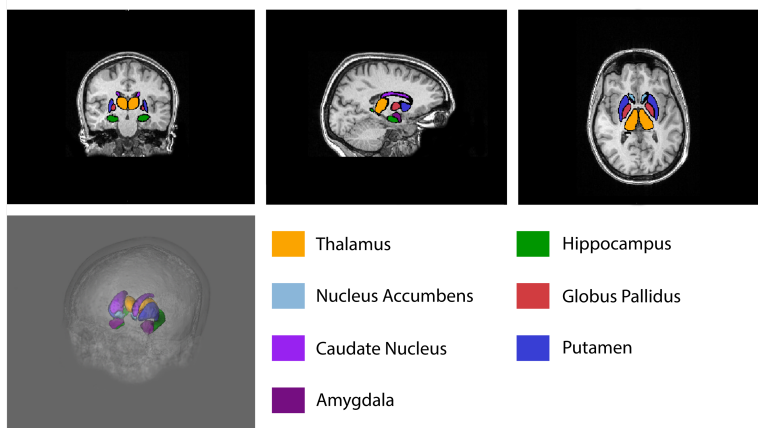
994 (A) Six Chinese symbols served as stimuli for the task and were associated with three values: two paired with reward, two
995 with loss and two with no financial change (neutral). (B) Representative trial of the learning phase. Symbols were displayed
996 for 1000ms, systematically paired with the corresponding (positive, negative or neutral) value, via visual and auditory
997 feedback. Characters presentation was alternated with a 1000ms fixation period. During the training phase, participants learned
998 associations between the stimuli and their reward value. C. Representative trial of the testing phase. After a 1000ms pretrial
999 interval, participants were primed with a 500ms preparatory cue signalling the upcoming stimuli. Two characters were then
1000 presented to the left and right hemifield, together with a spatial cue, instructing participants to covertly attend the symbol on
1001 the cued side (target) and ignore the other one (distractor). Participants' task was to report when the target stimulus changed
1002 contrast. Contrast change could either occur after 750ms (13% of trials), 1450ms (47% of trials) or 2350ms (40% of the trials).
1003 In 95% of the trials, the target changed contrast (valid trials), whilst in 5% of the trials, the distractor changed contrast (invalid
1004 trials). Figure adapted from [38].



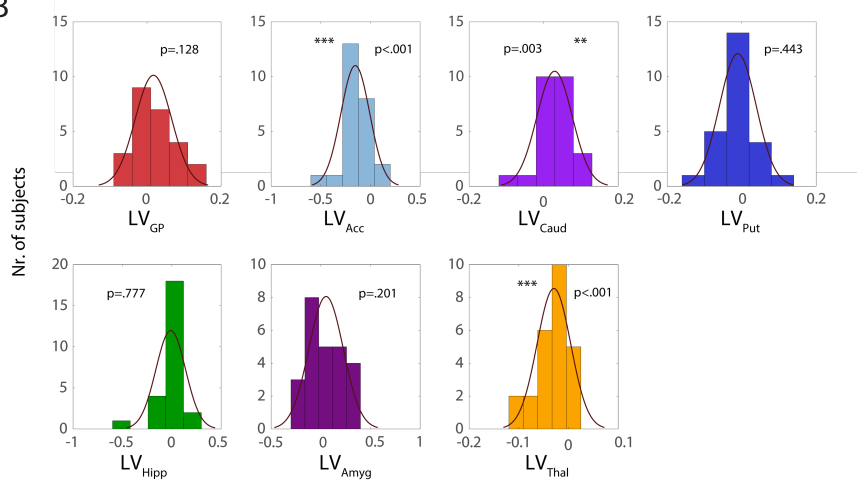
1005 **Figure 2. Grand average MI and HLM distribution across participants.**

1006 (A) Time-frequency representations of power (TFRs) and topographical plot showing contrast between the ‘attention right’ –
1007 ‘attention left’ trials. A clear modulation is visible at posterior sensors in the alpha band (8 – 13Hz) in the –750 – 0ms interval
1008 (this time window being considered for the computation of HLM(α) indices in (B)). Sensors included in the left and right ROIs
1009 are marked as dots. Trials are locked to the onset of the contrast change (t = 0). (B) Side panels show the temporal evolution
1010 of modulation indices in the alpha range (MI(α)), averaged over sensors within left and right hemisphere ROIs. The magnitude
1011 (absolute value) of MI(α) progressively increased in the stimulus interval until the onset of the contrast change. Middle:
1012 distribution of HLM(α) indices across participants, computed over the ROIs and 8 – 13 Hz frequency band (see Materials and
1013 Methods). A normal density function is superimposed, denoting no hemispheric bias in lateralized modulation values across
1014 participants (Shapiro Wilk, $W = .958, p = .392$).

A

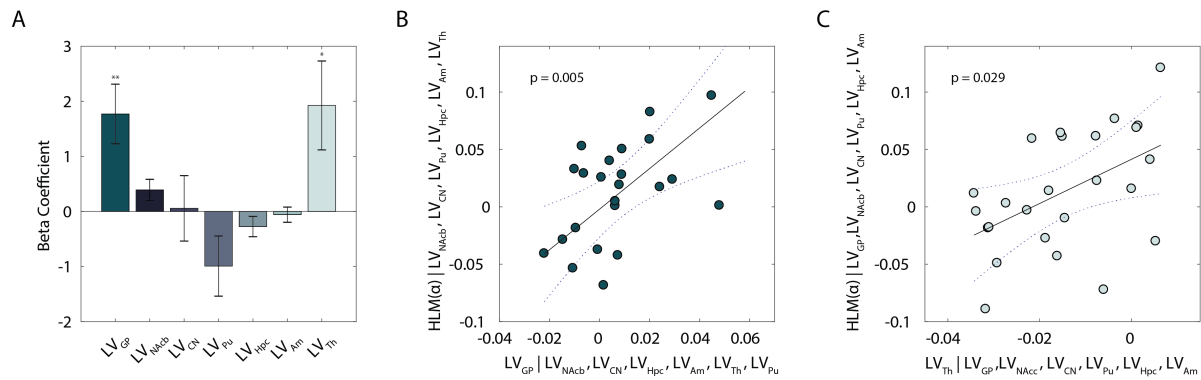


B

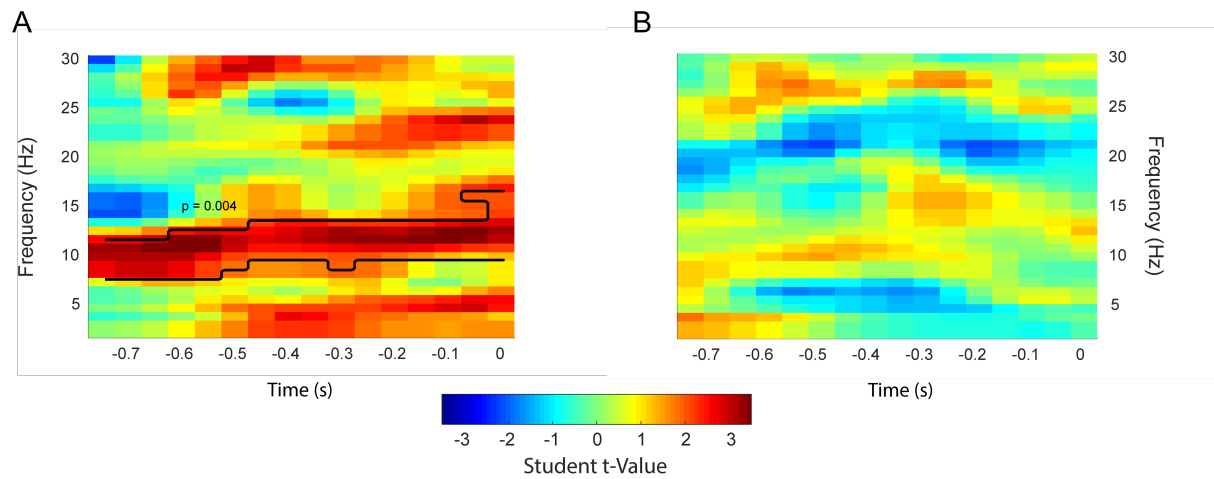


1015 **Figure 3. Basal Ganglia volumes resulting from semiautomated subcortical segmentation implemented.**

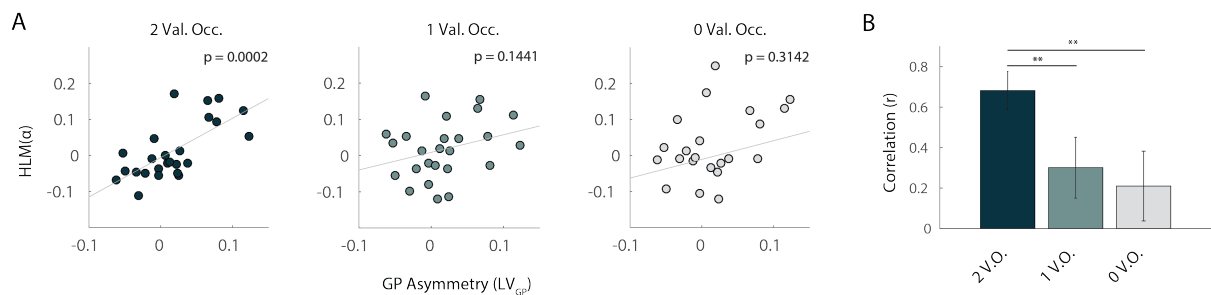
1016 (A) Orthogonal view and 3D rendering. Subcortical volumes are overlaid as meshes on the anatomical MRI of one of the
 1017 participants (following defacing procedure in Freesurfer, where voxels outside the brain mask with identifiable facial features
 1018 were excluded [103]). (B) Histograms with superimposition of normal density function, showing the distribution of subcortical
 1019 lateralization indices for each substructure. In our sample, NAcb and Th volumes were left lateralized ($p = .0001$ and $p = .0003$,
 1020 respectively) while CN showed a right lateralization ($p = .0029$).



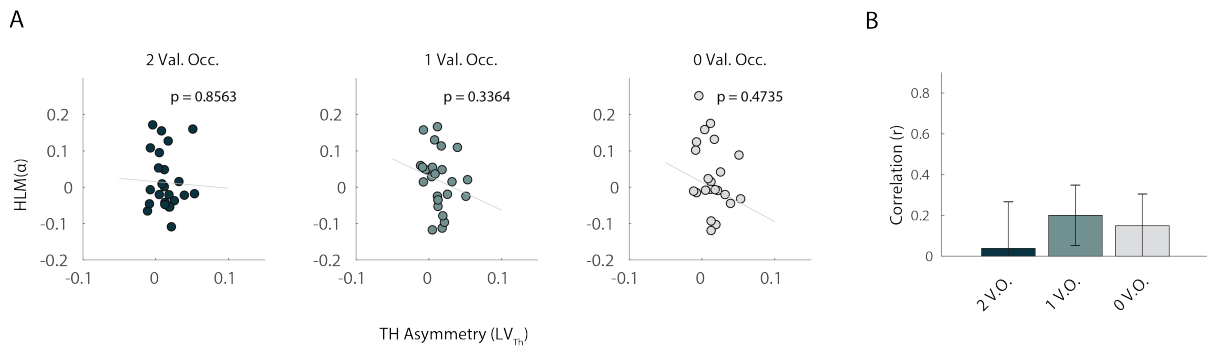
1021 **Figure 4.** Lateralization of individual subcortical structures in relation to alpha hemispheric lateralized modulation (HLM) in
 1022 the task. (A) Bar plot displays the Beta coefficients associated with a general linear model where LV values were defined as
 1023 explanatory variables for $HLM(\alpha)$. Error bars indicate standard error of the mean. Asterisks denote statistical significance;
 1024 $**p < .01$. (B) Partial regression plot showing the association between LV_{Gr} and $HLM(\alpha)$, while controlling for the other
 1025 regressors in the model in (A). (C) Partial regression plot showing the association between LV_{Th} and $HLM(\alpha)$, while controlling
 1026 for the other regressors in the model in (A). Given Eqs.(1) and (2) (see *Materials and Methods*), positive $HLM(\alpha)$ values
 1027 indicate stronger modulation of alpha power in the right compared to the left hemisphere, and vice versa; similarly, positive
 1028 (or negative) LV_s indices denote greater right(or left) volume for a given substructure s . The dotted curves in (B) and (C)
 1029 indicate 95% confidence bounds for the regression line, fitted on the plot in black.



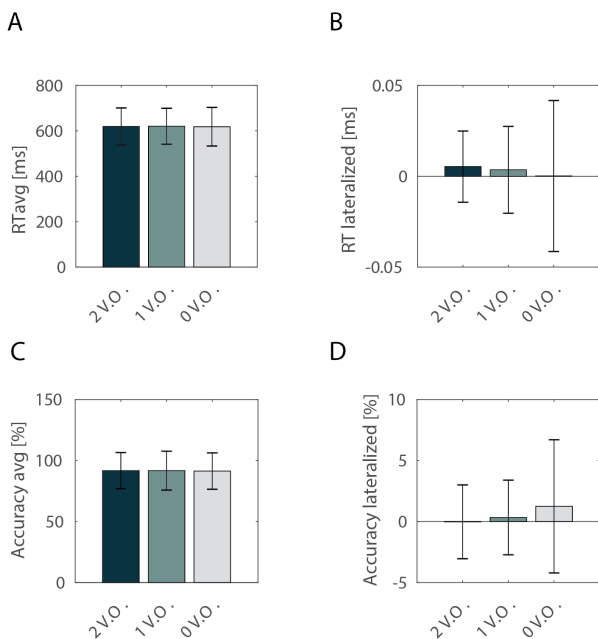
1030 **Figure 5.** Time-frequency representation of regression coefficient t-statistics on the linear relationship between lateralized
 1031 alpha modulation and LV_{GP} (A) and LV_{Th} (B) indices, averaged over ROIs (see Fig. 2A). A black outline is used to highlight
 1032 the significant time-frequency cluster found. For the LV_{GP} , the analysis revealed a clear α -band-limited association between
 1033 the variables across the full time-window of interest (see *Materials and Methods*).



1034 **Figure 6. Linear association between GP volumetric asymmetry and alpha modulation asymmetry as a function of**
 1035 **value-saliency occurrences in the task.** (A) Correlation between GP volume lateralization and $HLM(\alpha)$, grouped according
 1036 to the number of value-salient stimuli in the trials (see *Materials and Methods*). From left to right, respectively, two, one and
 1037 zero value-saliency occurrences are displayed. GP asymmetry significantly explained $HLM(\alpha)$ only when value-salient stimuli
 1038 featured as both target and distractors, irrespective of their valence ($r = .68$, significant at the $p < .001$ level after Bonferroni
 1039 correction for three comparisons). (B) The association between $HLM(\alpha)$ and GP volume lateralization increased as a function
 1040 of value saliency in the task: the linear relationship was stronger when two value-salient stimuli were presented, when
 1041 compared to conditions characterized by either one or value-saliency pairings (95% CI [.106, .672] and [.125, .897],
 1042 respectively for the two comparisons). This suggests that, when both target and distractor were associated with a salient value,
 1043 participants exhibiting bigger GP volume in the left hemisphere than in the right hemisphere, were also better at modulating
 1044 alpha oscillations in the left compared to the right hemisphere. Asterisks denote statistical significance; $**p < .01$.



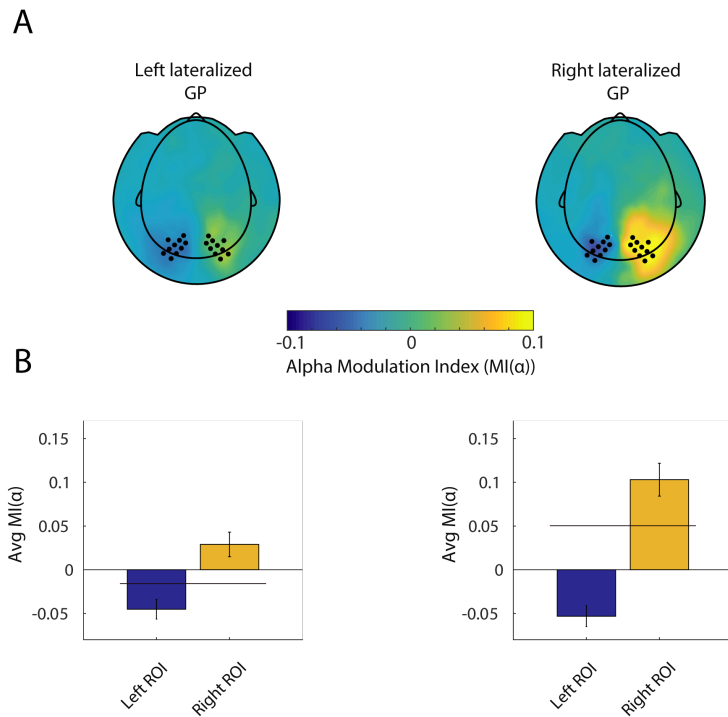
1045 **Figure 7. Linear association between Th volumetric asymmetry and alpha modulation asymmetry as a function of**
1046 **value-saliency occurrences in the task.** (A) Correlation between TH volume lateralization and HLM(α), grouped accordingly
1047 to the number of value-salient stimuli in the trials (see *Materials and Methods*). From left to right, respectively, two, one and
1048 zero value-saliency occurrences are displayed. When considering individual correlations between Th asymmetry and HLM(α),
1049 no significant linear relationship was found. (B) The association between the two measures also didn't significantly differ as
1050 a function of saliency in the trials.



1051 **Figure 8. Mean and lateralized reaction times (RT) and accuracy values across the three value-saliency occurrences in**
1052 **the task.**
1053 Mean RT (A) and accuracy (C) values averaged across participants in the three value-salient occurrences conditions in the
1054 task. Error bars indicate standard error of the means. No significant difference was found between groups by means of one-
1055 way repeated measures ANOVA, indicating that different levels of value-saliency pairings didn't influence behavioural
1056 performance. No significant difference emerged also when comparing average lateralized values of RT (B) and accuracy (D)
1057 across the same conditions, and by means of same statistical analysis, indicating that the behavioural spatial bias was not
1058 affected by the different levels of value-saliency pairings.

1059 **Supplementary material**

1060



1061 **Figure 1S. Alpha modulation indices for left and right hemispheres associated with two subgroups of the sample. (A)**

1062 Topographical plot of $MI(\alpha)$ values for the two participants groups, clustered according to directionality of GP lateralization

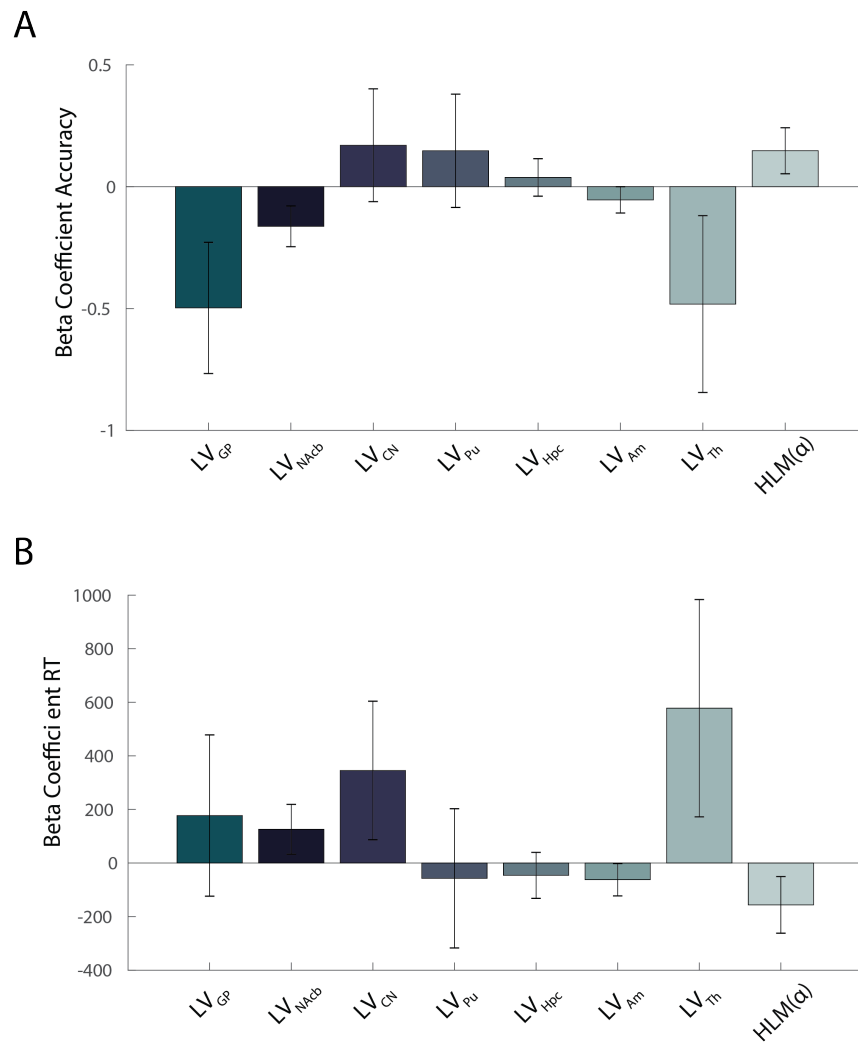
1063 (right vs left lateralized GP). Left and right sensors of interest are marked as dots and correspond to the same ROIs as in

1064 Figure 2. (B) Bar graph showing mean $MI(\alpha)$ averaged over ROIs in the two subgroups. As indicated in the cluster-based

1065 permutation results, a difference is particularly observable for right hemisphere alpha modulation between the two groups,

1066 being higher in participants exhibiting a right lateralized GP. Error bars represent standard error of the mean. Horizontal

1067 lines in the indicate the average $HLM(\alpha)$ indices for each subgroup.



1068 **Figure 2S.** General linear model displaying combined lateralized subcortical volumes and hemispheric lateralized
1069 modulation as multiple regressors for the prediction of spatial behavioural bias in accuracy (A) and RT (B). No significant
1070 regression was found which could account for either the lateralized accuracy or RTs ($p=.429$ and $p=.570$, respectively).